Mechanics of Materials 146 (2020) 103398

Contents lists available at ScienceDirect

Mechanics of Materials

journal homepage: www.elsevier.com/locate/mechmat

Research paper

Experimental and numerical analysis of the heat generated by plastic deformation in quasi-static uniaxial tensile tests

D.M. Neto[a,*], V.M. Simões[a,b], M.C. Oliveira[a], J.L. Alves[c], H. Laurent[b], A. Oudriss[d], L.F. Menezes[a]

[a] CEMMPRE, Department of Mechanical Engineering, University of Coimbra, Polo II, Rua Luís Reis Santos, Pinhal de Marrocos, Coimbra, 3030-788, Portugal
[b] Univ. Bretagne Sud, UMR CNRS 6027, IRDL, Lorient, F-56100, France
[c] CMEMS, Microelectromechanical Systems Research Unit, University of Minho, Campus de Azurém, Guimarães, 4800-058, Portugal
[d] LaSIE UMR CNRS 7356, La Rochelle Université, Avenue Michel Crépeau, 17042, La Rochelle, Cedex 1, France

ARTICLE INFO

Keywords:
Plastic deformation
Heat generation
Thermo-mechanical analysis
Taylor–Quinney coefficient
Uniaxial tensile test

ABSTRACT

This study evaluates the temperature variation observed in quasi-static uniaxial tensile tests, due to the heat generated by plastic deformation. The AA6016-T4 aluminium alloy was the material selected, considering different values of crosshead velocity (from 0.01 mm/s up to 1 mm/s). The temperature variation was also evaluated during the stress relaxation test. A finite element model of the uniaxial tensile test is presented, which takes into account the heat generated by plastic deformation, as well as the effect of the heat losses to the environment (convective heat transfer coefficient) and to the grips (interfacial heat transfer coefficient). The numerical results show that the predicted temperature variation is almost independent of the selected heat transfer coefficients. On the other hand, the temperature rise is influenced by the Taylor–Quinney coefficient. The comparison between experimental and numerical temperatures shows that the Zehnder model (increasing Taylor–Quinney coefficient) provides more accurate results than the Aravas model (decreasing Taylor–Quinney coefficient). Nevertheless, the evolution of the Taylor–Quinney coefficient defined by the Zehnder model assumes a constant value for the hardening coefficient, which does not fit the hardening behaviour observed for this aluminium alloy.

1. Introduction

In sheet metal forming processes, the blank temperature increases during the forming operation due to the heat generated by plastic deformation and by friction between the blank and the forming tools (Pereira and Rolfe, 2014). This is particularly relevant in mass production lines due to the periodic input of heat into the forming tools. In fact, the temperature variation produces changes both in the mechanical behaviour of the blank and particularly in the lubrication conditions, contributing to process variability (Hazra et al., 2011). Therefore, this phenomenon should be considered during the optimization of the process parameters, mainly in case of high strength steels and for high speed forming operations. Hence, the accurate numerical modelling of these forming processes requires a thermo-mechanical analysis, to account for the influence of the heat generated by plastic deformation.

Since the deformation process of metallic materials in the elastic regime leads to insignificant volume changes (lower than 1%), the temperature variation defined by the Joule–Thomson effect for solids is always slight (Kuo et al., 2005). In contrast, the plastic deformation generates a significant amount of heat (Farren and Taylor, 1925), which can lead to substantial temperature increases if the deformation process is fast (no time for heat exchange). Indeed, during plastic deformation, the mechanical energy is predominantly dissipated as heat, while the stored or latent energy remains in the material after removing the external loads (Hodowany et al., 2000). The first attempts to determine experimentally the fraction of plastic work converted into heat was carried by Taylor and Quinney (1934), using calorimetric methods. They found that the fraction of dissipated energy (also known as Taylor–Quinney coefficient) is about 90% for different metallic materials.

Some experimental studies show that the Taylor–Quinney coefficient may depend on the plastic strain and on the plastic strain rate. The study performed by Macdougall (2000) on an aluminium alloy shows that the Taylor–Quinney coefficient increases with the plastic strain, ranging roughly from 0.5 to 0.9, which is in agreement with the model developed by Zehnder (1991). An identical tendency was found by Rusinek and Klepaczko (2009) for TRIP steels, taking into account the

* Corresponding author.
E-mail addresses: diogo.neto@dem.uc.pt (D.M. Neto), vasco.simoes@uc.pt (V.M. Simões), marta.oliveira@dem.uc.pt (M.C. Oliveira), jlalves@dem.uminho.pt (J.L. Alves), herve.laurent@univ-ubs.fr (H. Laurent), abdelali.oudriss@univ-lr.fr (A. Oudriss), luis.menezes@dem.uc.pt (L.F. Menezes).

https://doi.org/10.1016/j.mechmat.2020.103398
Received 18 July 2019; Received in revised form 9 February 2020; Accepted 16 March 2020
Available online 19 March 2020

phase transformation of austenite into martensite during plastic deformation. On the other hand, the influence of the plastic strain rate on the Taylor–Quinney coefficient was experimentally studied by Zhang et al. (2017), using the Kolsky bar with an infrared temperature measurement system. For the 7075-T651 aluminium alloy, they found that the Taylor–Quinney coefficient increases from 0.4 to 0.9 as the strain rate increases from 1100 to 4200 s^{-1}. Nonetheless, a different conclusion was obtained by Hodowany et al. (2000) for the 2024-T3 aluminium alloy, showing that the fraction of plastic work dissipated as heat is not sensitive to the strain rate over a range from 1 s^{-1} to 3000 s^{-1}. Recently, the dependence of the Taylor–Quinney coefficient on the dynamic loading mode (tension, compression and shear) was experimentally studied by Rittel et al. (2017). The results show that identical coefficients are measured in tension, compression and shear, except for the commercially pure titanium, which is known to exhibit tension − compression asymmetry in its mechanical properties (Revil-Baudard et al., 2015).

In order to take advantage of the adiabatic conditions, high strain rate techniques (e.g. the Kolsky pressure bar) are commonly adopted to calculate the fraction of plastic work converted into heat, where the amount of heat generated is captured by infrared temperature measurements (Mason et al., 1994). Alternatively, hybrid approaches have been developed, combining experimental measurements with numerical analysis through inverse analysis (Zehnder et al., 1998). These approaches are particularly attractive in mechanical tests involving low and intermediate strain rates, i.e. loading under non-adiabatic conditions. The hybrid method developed by Pottier et al. (2013) combines full field measurements (strains and temperature) on heterogeneous tensile tests with numerical results of the thermo-mechanical finite element analysis. They use a Levenberg–Marquardt algorithm to optimize sequentially the mechanical parameters and the Taylor–Quinney coefficient.

The experimental techniques used for temperature measurement can be categorized into two groups: (i) contact and (ii) non-contact techniques. The temperature variations induced by plastic deformation are commonly measured using thermocouples (contact technique) or infrared thermography (non-contact technique) (Ait-Amokhtar et al., 2008). Compared to thermocouples, infrared thermography has the advantage of providing the thermal image of the surface under investigation, while thermocouples measure the temperature on a single point. Therefore, infrared thermography is commonly used to study local temperature variations, such as the ones associated with the Portevin–Le Chatelier effect of Al–Mg alloys (Ait-Amokhtar et al., 2008; Bernard et al., 2013). On the other hand, thermocouples can be inserted in the specimen, allowing the temperature measurement in hidden regions, which is very useful for some experimental studies (Pereira and Rolfe, 2014). Thermocouples spot welded on the specimen surface were reported to present a response time of about 10 milliseconds (Pandey and Chand, 2003), but response times of 10 microseconds can be attained in case of thermocouples embedded in the specimen (Rittel, 1998). Infrared thermography cameras have a response time between milliseconds and microseconds, for cameras based on thermal detectors and on quantum detectors, respectively (Carlomagno and Cardone, 2010). Finally, although the temperature measurement with both systems depends on the working conditions, infrared thermography also requires the calibration of the surface emissivity, which can change during plastic deformation (Hodowany et al., 2000). In order to minimize emissivity problems, the specimen surface is often painted with a high-emissivity graphic-black coating (Ait-Amokhtar et al., 2008; Bernard et al., 2013).

The purpose of this paper is to use temperature variation measurements from *quasi*-static uniaxial tensile tests to quantify the fraction of plastic work converted into heat. The accuracy of the numerical models that take into account the Taylor–Quinney coefficient as a function of plastic strain is evaluated. The material and the experimental setup of the *quasi*-static uniaxial tensile tests used are described in Section 2, while the experimental results are presented in Section 3. The proposed thermo-mechanical finite element model is presented in Section 4 including, both the heat generation and the heat losses that occur during the test. The comparison between numerical and experimental temperature results is performed in Section 5, highlighting the influence of the Taylor–Quinney coefficient on the predicted temperature. Section 6 contains the main conclusions of this study.

Table 1
Chemical composition of the AA6016-T4, in percent composition by mass (wt. %), (supplier results).

Si	Mg	Cu	Fe	Mn
0.91	0.41	0.10	0.255	0.17

2. Experimental methods and apparatus

2.1. Material

The age-hardenable aluminium alloy AA6016-T4 was adopted for this study, in sheet format with a thickness of 1.05 mm. The chemical composition of the alloy AA6016-T4 is presented in Table 1. The designation T4 is associated with the following sequence: solution heat treatment (SHT), rapid quenching and natural aging to a substantially stable condition. The mechanical behaviour of the alloy was evaluated after 1, 7 and 18 months of natural aging by Simões et al. (2019). The results show that the mechanical strength increased with the storage time at room temperature, phenomenon known as natural aging effect. The mechanical properties are presented in Table 2, as a function of the natural aging time, highlighting the fact that they remain stable after a storage time of 7 months. Concerning the anisotropy coefficients, their evolution with natural aging was negligible (Simões et al., 2019). The normal anisotropy coefficient (r_n) is equal to 0.615 and the planar anisotropy coefficient (Δr) is equal to 0.030, which indicates that the in-plane variation of the anisotropy coefficient is negligible.

The microstructural characterization of the as-received material, after 18 months of natural aging, was performed by SEM – Scanning Electron Microscopy (FEI Quanta 200 ESEM-FEG) coupled to Electron Back Scatter Diffraction (EBSD EDAX/TSL OIM system). An accelerating voltage of 20 kV was chosen to obtain optimum diffraction condition. Automatic beam scanning and the TSL OIM Data Collection 5 software were used to map the crystal orientations on planar sections. The samples surface for the EBSD analyses was prepared by grinding to 1000, 2400 and 4000 grit silicon carbide papers, followed by cloth polishing in 1 and ¼ μm diamond suspension. Finally, a surface finishing was carried out by vibrating polishing using colloidal silica (particle size ~ 0.02 μm) for 2 h. These steps of the surface preparation procedure allow to obtain Kikuchi patterns with high resolution. Each EBSD map typically consists of 200–400 grains. The EBSD analyses

Table 2
Mechanical properties of the AA6016-T4 evaluated at different values of natural aging time (Simões et al., 2019).

aging time	$R_{p0.2}$ [mpa]	R_m [mpa]	A_g [%]	$n_{4\text{-}6}$	$n_{10\text{-}15}$
4 days*	88	198	25	0.32	0.27
1 month	101	218	24	0.32	0.26
7 months	126	237	23	0.29	0.25
18 months	127	237	23	0.29	0.25

The terms and definitions used throughout this work are according to (ISO 6892-1: 2009) (i.e. R_m tensile strength; $R_{p0.2}$ proof strength at 0.2% of the extensometer gauge length; A_g percentage of non-proportional elongation at maximum force) and the (ISO 10275:2007) (i.e. the strain hardening exponent (n), which in this case was evaluated between 4 and 6% of plastic deformation, n_{4-6}, and 10 and 15%, n_{10-15}).

* supplier results.

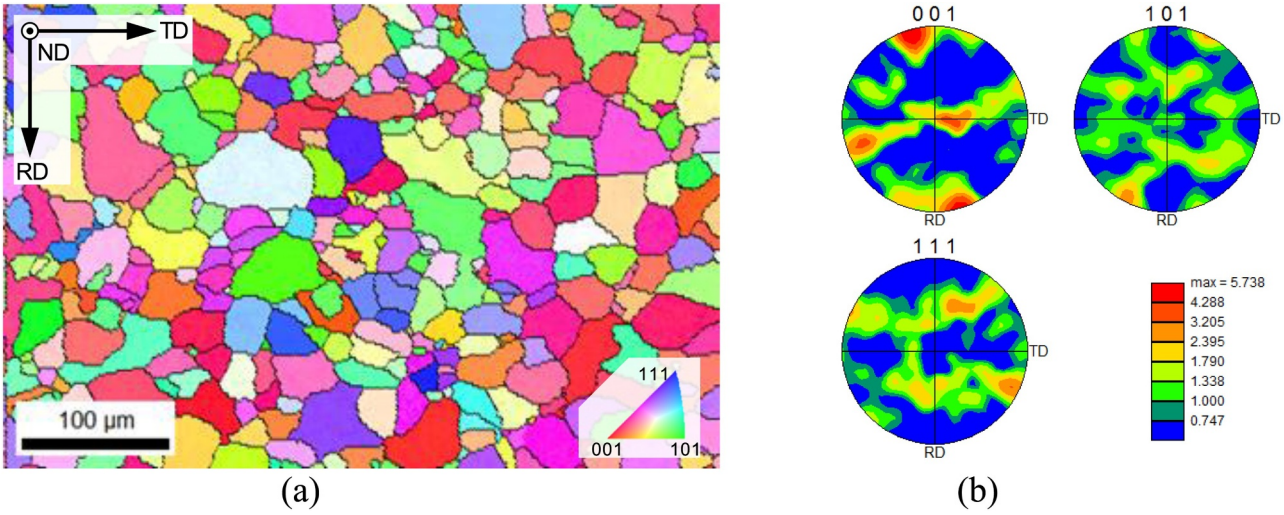

Fig. 1. EBSD analysis of the material, after 18 months of storage time: (a) grain microstructure (inverse pole figure maps); (b) direct pole figures.

were performed considering a minimum step size of 1 μm.

The EBSD measurements shown in Fig. 1 were performed on the plane of the sheet, i.e. in the RD-TD plane (RD: rolling direction; TD: transverse direction) which is perpendicular to the normal direction (ND). As shown in Fig. 1(a), the material presents equiaxed grains, which have an average grain size diameter of around 32 μm, with a standard deviation of 12 μm. The direct pole figures show a slight preferential crystallographic texture {001} <100> (see Fig. 1(b)). These results are in agreement with a previous study for the A6016-T4 alloy, which confirms that after the SHT the material presents a fully recrystallised microstructure, composed of grains with an average grain size of about 30 μm, slightly elongated along the RD. Moreover, its texture is dominated by a characteristic cube orientation {001} <100> at (0°,0°,90°) with pronounced scatter about the RD towards Goss {011} <100> at (0°,45°,90°) (Engler et al., 2015).

The physical and thermal properties are given in Table 3. The mass density and the specific heat are the values globally accepted for aluminium alloys, which were obtained from the literature (Mills, 2002). On the other hand, the thermal conductivity was determined by the Wiedemann–Franz law using the experimental measurement of the electrical conductivity ($25.75 \times 10^6\ \Omega m^{-1}$). The electrical conductivity was measured at room temperature by four-point probe technique (Smits, 1958), using the device FISCHERSCOPE MMS PC2.

2.2. Uniaxial tensile tests

The bone shaped specimen was adopted to perform the uniaxial tensile tests, considering the dimensions presented in Fig. 2(a). The width and the nominal length of the parallel gauge section are 10 mm and 40 mm, respectively. All the specimens were cut from the received sheets using a wire-cut EDM machine, ensuring the dimensional accuracy and the surface finish.

The tensile tests were performed on a thermo-mechanical testing machine Gleeble 3500, which is equipped with input temperature channels for thermocouples. More details about both the control system and the mechanical drive system of this machine can be found in Fekete and Szekeres (2015). This machine is classically used to perform

Table 3
Physical and thermal properties of the AA6016-T4 alloy.

Mass density (ρ) [kg/m^3]	Specific heat (c_p) [J/kg°C]	Thermal conductivity (k) [W/m°C]
2800	850	184

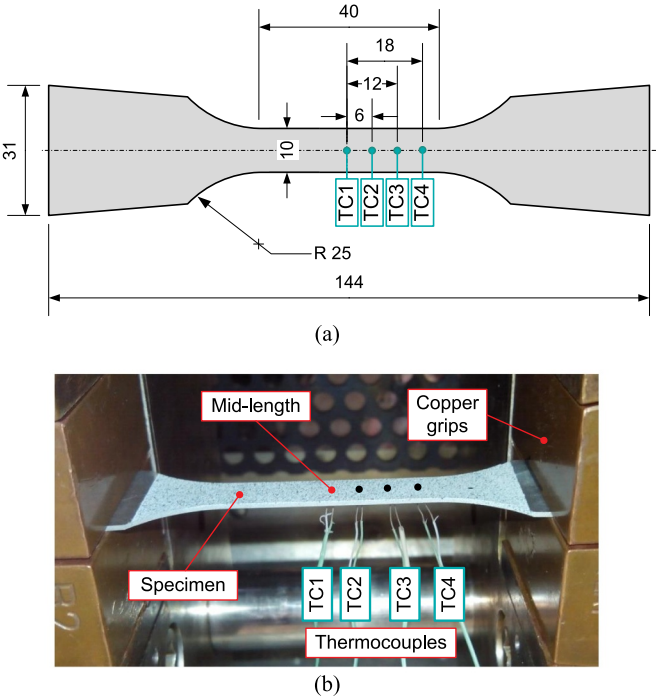

Fig. 2. Uniaxial tensile test, with or without stress relaxation stages, on the Gleeble machine: (a) specimen geometry and thermocouples position (dimensions in mm); (b) experimental setup.

tensile tests with control of temperature as presented in Manach et al. (2016), in which the temperature influence on the mechanical behaviour was studied for the alloys AA6016-T4 and AA6061-T6. The same equipment was used to characterize the mechanical behaviour of the AA6016-T4 alloy through uniaxial tensile tests, performed at room temperature, under monotonic load until rupture. These tests were carried out using displacement control with prescribed crosshead velocities of 0.01 mm/s, 0.1 mm/s and 1 mm/s. Consequently, three different average values of strain rates are obtained depending on the prescribed crosshead velocity, which corresponds to the strain rates of $2 \times 10^{-4}\ s^{-1}$, $2 \times 10^{-3}\ s^{-1}$ and $2 \times 10^{-2}\ s^{-1}$. Additionally, for the crosshead velocity of 0.1 mm/s, tensile tests were performed at 0°, 45°, and 90° to the sheet RD. All these tests were performed for 1 and 18 months of natural aging. The strain rate arising in the metal sheet during the forming processes is mainly defined by the

part geometry and the punch speed. Considering the cylindrical cup test proposed by Manach et al. (2016), numerical results indicate that for 5 mm/s of punch speed the maximum strain rate value is about 0.1 s^{-1} (Neto et al., 2018). Besides, assuming a strain rate insensitive material, the increase (decrease) of the punch speed leads to a proportional increase (decrease) of the strain rate values.

The same experimental apparatus and specimen geometry were used to perform uniaxial tensile tests with stress relaxation stages, restricted to the aluminium alloy with 18 months of natural aging. In this tensile stress relaxation test, the specimen is stretched with a crosshead velocity of 0.1 mm/s during 30 s, followed by a stress relaxation time of 60 s. This loading cycle followed by a relaxation period is performed 3 times, i.e. the total testing time is 270 s. For each test condition previously described, at least two tensile tests were performed. The average scatter of the stress was less than ± 1 MPa for the same strain value, which confirms the reproducibility.

2.3. Measurement techniques

The layout of the experimental apparatus used to perform the tests is presented in Fig. 2(b), highlighting the specimen mounted in the copper grips. The temperature evolution was measured using thermocouples, while the strain evolution was measured by an optical Digital Image Correlation (DIC) system synchronized with the Gleeble system. The cameras of DIC system were placed above the specimen gauge area, while the thermocouples were welded on its backside surface (see Fig. 2(b)).

The DIC system used was Aramis-4 M (GOM mbH) that, based on triangulation, provides precise 3D coordinates for full-field and point-based measurements, which allows the measurement of 3D surface strain with an accuracy up to 0.01% (GOM mbH 2009). Two video cameras with a resolution of approximately 30 pixels/mm^2 (2358 × 1728 pixels in the measurement area of 80 × 55 mm^2) recorded the motion of the specimen surface at the maximum frequency of 60 Hz. The Hencky strain tensor components were calculated by averaging the full field measurements of a rectangular shape with 35 mm length and 8 mm width, centred in the specimen gauge zone. The selected dimensions were slightly lower than the gauge area in order to minimize the influence of border effects. Finally, the frequency of acquisition used in the Aramis-4 M system was selected according to the crosshead velocity. Hence, the selected frequencies were 1 Hz, 5 Hz and 50 Hz, for 0.01 mm/s, 0.1 mm/s and 1 mm/s of crosshead velocity, respectively.

The temperature evolution was measured using type-K thermocouples (wire diameter of 250 μm) which were welded on the specimen surface (exposed). As shown in Fig. 2(a), the thermocouples were welded at the specimen middle (TC1), 6 mm from mid-length (TC2), 12 mm from mid-length (TC3) and 18 mm from mid-length (TC4). However, in the tests performed with 1 month of natural aging only one thermocouple (TC1) was used. The selected frequency of acquisition for the temperature was 5 Hz, 50 Hz and 100 Hz, for 0.01 mm/s, 0.1 mm/s and 1 mm/s of crosshead velocity, respectively. It should be mentioned that, whenever the temperature is plotted as a function of strain, the results are plotted considering the lower acquisition frequency of the DIC system.

The entire welding procedure of the thermocouples is shown in Fig. 3, which can be divided into three steps. First, the two thermocouple cables are welded together (see Fig. 3(a)). Second, the oxidation of the surfaces of the thermocouple and of the sheet was removed by local sandblasting (see Fig. 3(b)). Third, the thermocouple was welded on the specimen using a 35,200 Thermocouple Welder, from Dynamic System Inc (Gleeble Systems), using a welding voltage of 45V-DC (see Fig. 3(c)). After welding each thermocouple on the specimen surface, its temperature measurement was controlled and validated before performing the test. The local influence of the thermocouple and the weld spot can be considered irrelevant in the mechanical properties of the specimen, as shown in Fig. 3(d). Indeed, the rupture of the specimen never occurs in the weld zone. Fig. 3(e) shows that after removing the thermocouple from the sample, the material of the thermocouple stays in the sheet and vice versa, showing the good adhesion of the thermocouple to the sheet.

The thermocouples were connected to the acquisition system of the Gleeble device, which measures the temperature with a resolution of about 1 × 10^{-5} °C. Thermocouples of type-K have a standard accuracy of 2.2 °C (Omega Engineering Inc 2010). In order to minimize the impact of the accuracy in the results analysis, the values presented throughout this work correspond to the variation of the temperature relatively to the temperature measured by each thermocouple at the beginning of the tensile test, i.e. temperature variation.

The precision of the temperature variation was evaluated based on experiments carried out with two specimens tested under the same conditions. This evaluation was based on the difference of the temperature variation during the tests, for thermocouples located in the same position along the specimen length. The precision determined for the temperature variation was evaluated as inferior to ± 0.1 °C. The temperature variation measured by different thermocouples in the same specimen, while it is kept undeformed, was used to evaluate the noise amplitude. The noise amplitude in the temperature variation is inferior to 0.2 °C, and approximately constant during time interval used in the analysis. More details concerning the uncertainty in temperature measurements are given in Appendix A: Temperature measurements.

3. Experimental results

3.1. Uniaxial tensile tests

The stress–strain curves obtained from the uniaxial tensile tests performed at crosshead velocities of 0.01, 0.1 and 1 mm/s, with the specimens oriented along the RD and aging times of 1 month and 18 months, are presented in Fig. 4. The increase of the natural aging time leads to an increase in the alloy strength (Simões et al., 2019). Moreover, the increase of the crosshead velocity leads to negligible differences in the flow stress curves. Therefore, this aluminium alloy can be assumed strain rate insensitive at room temperature (Simões et al., 2019).

Fig. 5 shows the temperature variation in the specimen middle (TC1) as a function of strain, for the tests presented in Fig. 4. As shown in Fig. 5, when the tensile specimen is loaded, the temperature decreases during the elastic regime and then increases during the elasto-plastic one. The temperature drop occurs due to volume changes caused by elastic deformation (Joule–Thomson effect) and is approximately 0.25 °C for this aluminium alloy, as highlighted in the zoom in Fig. 5. The temperature increase occurs due to heat generated by plastic deformation, and its increase depends of the crosshead velocity used. In fact, although the heat generated by plastic deformation is not influenced by the crosshead velocity (strain rate insensitive material as shown in Fig. 4), both the heat losses and the thermal conduction are time dependent. Thus, increasing the crosshead velocity leads to a global increase in the temperature due to the lower time to dissipate the heat generated by plastic deformation (Gao and Wagoner, 1987). Considering the material with 18 months of natural aging, the temperature rise was around 0.2, 2 and 10 °C for the crosshead velocities of 0.01, 0.1 and 1 mm/s, respectively. Especially at a crosshead velocity of 1 mm/s, the natural aging time leads to an increase of the temperature rise due to the higher flow stress (see Fig. 4), which increases the amount of heat generated by plastic deformation in the same proportion of the stress increase. Finally, the temperature increase observed due to plastic strain is similar to the one reported by Bernard et al. (2013), under quasi-static uniaxial tensile tests at strain rates of 2 × 10^{-3} s^{-1} and 1 × 10^{-2} s^{-1}, for the AA5754-O aluminium alloy, which has a similar hardening behaviour.

The evolution of the experimental temperature variation with time

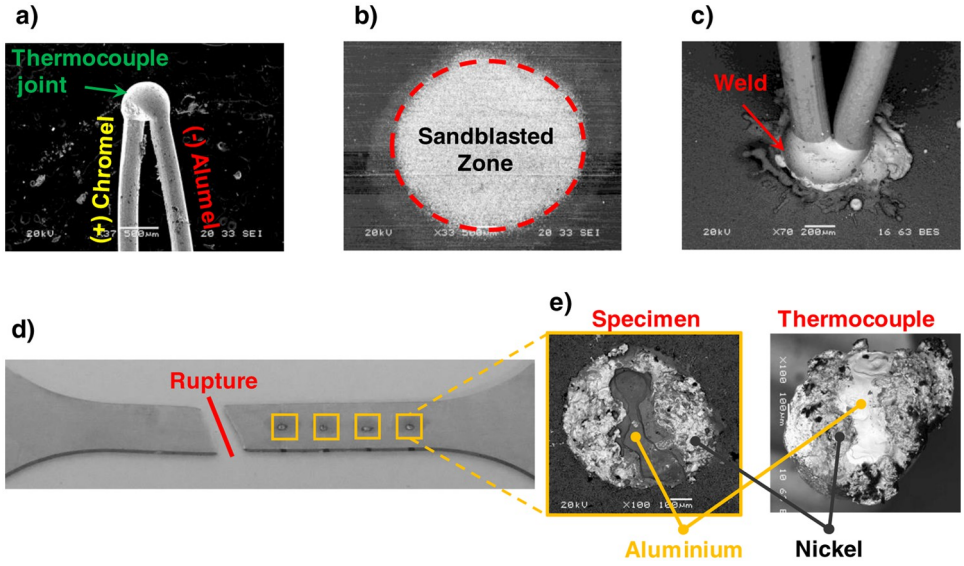

Fig. 3. Welding of the thermocouples on the tensile specimens: (a) welding thermocouple cables together; (b) sheet sandblasted zone; (c) thermocouple welded on the specimen; (d) specimen after tensile test; (e) sample and thermocouples after removal.

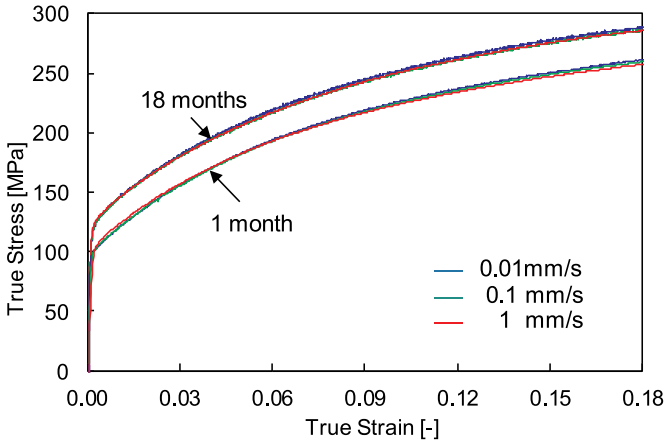

Fig. 4. Experimental true stress–true strain curves obtained from uniaxial tensile tests, performed at three different values of crosshead velocity (1 month and 18 months of natural aging).

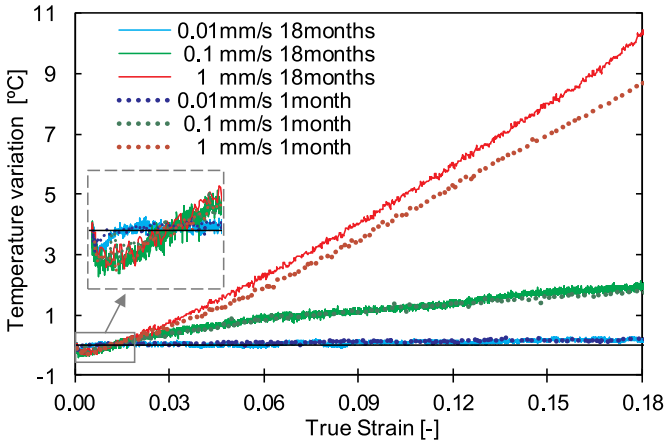

Fig. 5. Experimental temperature variation at the midpoint (TC1) of the tensile specimen (prior to the onset of necking) for different values of crosshead velocity, comparing 1 month and 18 months of natural aging. A zoom is presented to highlight the elastic regime.

for the four thermocouples is shown in Fig. 6, for specimens aged for 18 months. The results are presented for the grip velocities of 0.01, 0.1 and 1 mm/s, prior to the onset of necking, which is attained at approximately 1000, 100 and 10 s of the test time, respectively. Since the four thermocouples are positioned along the specimen length (see Fig. 2), it is possible to evaluate the temperature gradient. Globally, the temperature variation is always higher in the thermocouple placed at the specimen centre (TC1), which highlights the effect of heat conduction from the specimen to the grips. Indeed, the gradient of the temperature variation along the specimen length is dictated by the equilibrium between the heat generated by plastic deformation and the heat losses. The heat is generated mainly in the gauge section of the specimen (zone with plastic deformation), while the heat loss is prevalent at the contact interface with the copper grips. Therefore, comparing the four thermocouples, the temperature variation decreases from TC1 to TC4. For 10 mm of grip displacement (corresponding to a strain of 0.172), the difference in temperature variation between TC1 to TC4 is about 0.17 °C, 0.70 °C, and 4.14 °C for the grip velocity of 0.01 mm/s, 0.1 mm/s and 1 mm/s, respectively.

The experimental stress–strain curves obtained from uniaxial tensile tests performed at 0°, 45° and 90° to RD are presented in Fig. 7, for the material with 18 months of natural aging. The flow stress is slightly higher for RD but, globally, the in-plane variation of the flow stress is negligible. As previously mentioned in Section 2.1, the planar anisotropy coefficient is also very low (0.03). Thus, the plastic behaviour of this aluminium alloy can be modelled assuming planar isotropy.

The temperature variation measured in the midpoint of the specimen (TC1) is also presented in Fig. 7, for the same three uniaxial tensile tests. The influence of the loading direction used in the uniaxial tensile tests (0°, 45° and 90°) on the measured temperature is negligible, which is coherent with the planar isotropy assumption. The temperature variation is slightly higher for the test performed with the specimen aligned along the RD, since the flow stress is also higher in the RD, particularly for large values of strain. Although these uniaxial tensile tests were not performed under the same conditions (three different in-plane directions), this analysis allows highlighting the high reproducibility of both the temperature variation and the stress evolutions.

3.2. Stress relaxation tests

In the context of this work, the main goal of the stress relaxation test

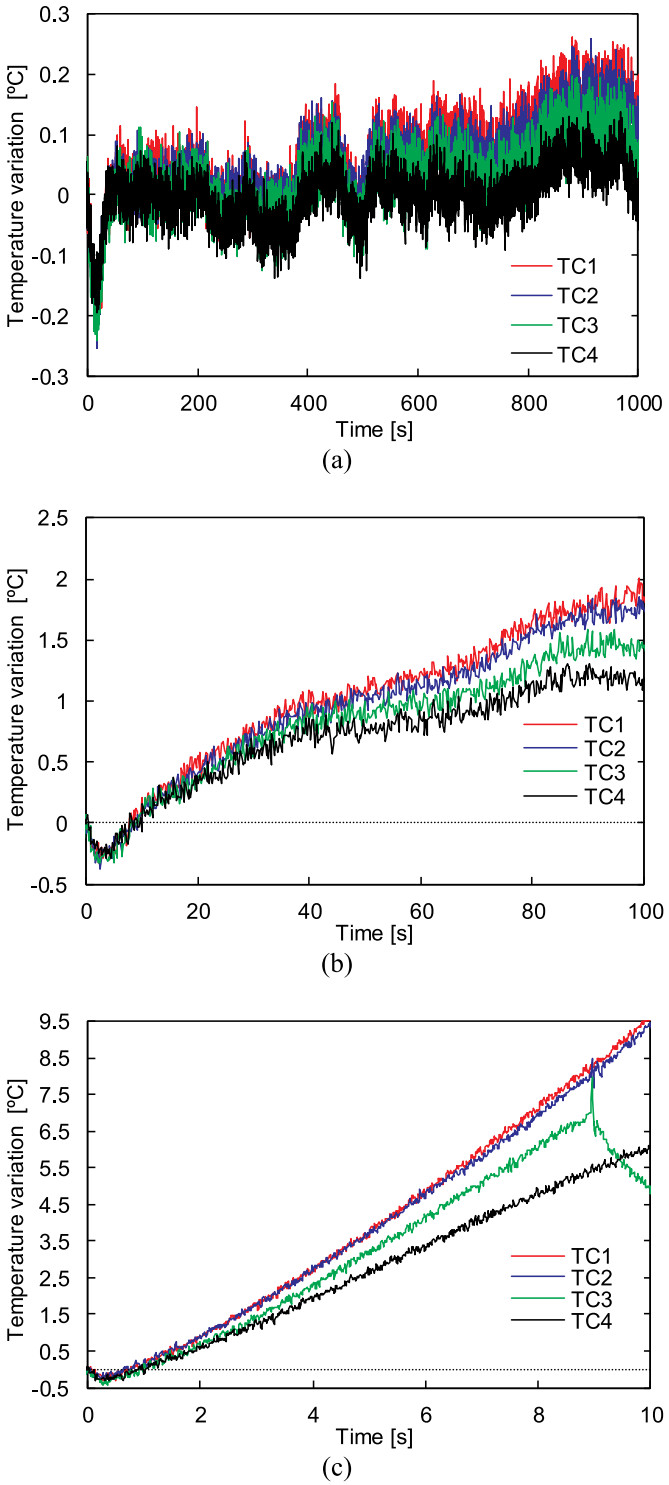

Fig. 6. Experimental temperature variation at 18 months of natural aging, measured by four thermocouples for crosshead velocity: (a) 0.01 mm/s; (b) 0.1 mm/s; (c) 1 mm/s. (Note: For crosshead velocity of 1 mm/s, the thermocouple TC3 broke up after 9 s of the tensile test).

is the analysis of the temperature variation and its connection with the mechanical response of the material. Fig. 8(a) presents the grip displacement imposed during the test, as well as the evolution of the stress as a function of time (18 months of natural aging). The stress increases during the stretching periods and decreases during the relaxation stages. The amount of stress decay, which occurs under a constant value of strain in the relaxation stage, increases in each stress relaxation

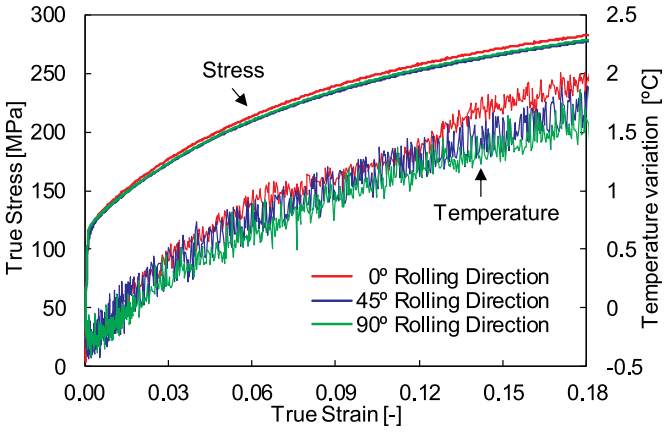

Fig. 7. Experimental true stress–true strain curves and temperature variation (measured in TC1) obtained from uniaxial tensile tests at 1 mm/s of crosshead velocity in three different directions with RD (18 months of natural aging).

stage, i.e. as the specimen is stretched. Despite the stress relaxation behaviour, the stress–strain curve obtained from the uniaxial stress relaxation test is identical to the monotonic stress–strain curve, as shown by Simões et al. (2019) for the same aluminium alloy (1 month of natural aging). However, after each stress relaxation stage, the stress value suddenly increases attaining a local maximum and then stabilizes into a plateau ending up by recovering the monotonic behaviour and without significant change of the material behaviour (see Fig. 8(a)). The stress jump occurs associated with the presence of Lüders bands, which also justify the plateau, as shown by Simões et al. (2019) for the same aluminium alloy (1 month of natural aging).

The temperature variation of the four thermocouples during the tensile stress relaxation test is presented in Fig. 8(b). Globally, in each load stage the temperature rises due to the plastic deformation of the material, while in each relaxation stage the temperature drops due to heat losses (conduction to the grips and natural convection with the surrounding environment). In the relaxation stages, the temperature drops to the room temperature since the relaxation period of 60 s allows the specimen to attain the thermal equilibrium. Therefore, each load stage starts at a similar initial temperature. The temperature rise increases at each load cycle when compared with the previous one, due to the material strain hardening.

4. Finite element model

Despite the uniaxial tensile tests are carried out at room temperature, the specimen temperature increases due to the heat generated by plastic deformation. Therefore, numerical simulation should address the thermo-mechanical analysis of the process (Martins et al., 2017). The numerical simulations were carried out with the in-house finite element code DD3IMP (Menezes and Teodosiu, 2000), which has been developed to simulate sheet metal forming processes (Oliveira et al., 2008). Only an eighth of the tensile test is simulated due to geometric and material symmetry conditions (see Fig. 2(a)). The specimen geometry (1/8) was discretized with eight-node hexahedral finite elements using a structured mesh composed by 1600 elements. The thermal problem considers full integration, while the mechanical problem uses selective reduced integration (Hughes, 1980) to avoid volumetric locking.

4.1. Constitutive modelling

The effect of the temperature on the material mechanical behaviour is not taken into account in the present model. Indeed, the thermo-mechanical coupling is assumed unidirectional, i.e. the predicted temperature field is affected by the mechanical solution, but the

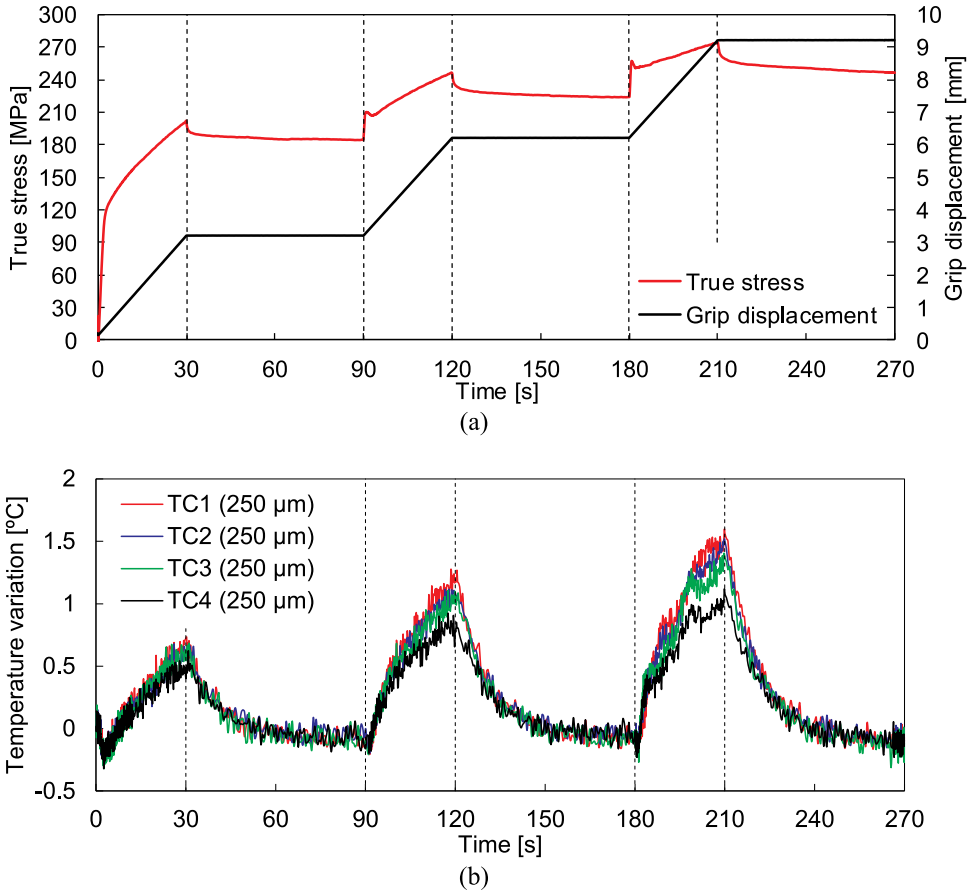

Fig. 8. Stress relaxation tensile tests carried out at 0.1 mm/s crosshead velocity on a sample with 18 months of natural aging: (a) true stress and grip displacement curves in the function of time; (b) temperature variation curves in the function of time.

mechanical behaviour is not affected by the temperature. This assumption results from the fact that the maximum temperature rise is about 10 °C for the highest strain rate considered. Since this alloy is strain rate insensitive at room temperature (see Fig. 4), a rate-independent elastoplastic model is used to describe the specimen deformation. Besides, the elastic behaviour is considered isotropic and modelled by the generalized Hooke's law with $E = 69$ GPa and $\nu = 0.33$. Regarding the plastic behaviour of this aluminium alloy, it is assumed non-linear with transverse isotropy.

The flow stress of the AA6016-T4 aluminium alloy is defined by the phenomenological Voce hardening law. Thus, the isotropic work hardening is described by:

$$Y = Y_{sat} - (Y_{sat} - Y_0)\exp(-C\bar{\varepsilon}^p), \quad (1)$$

where $\bar{\varepsilon}^p$ represents the equivalent plastic strain, Y_0 denotes the initial yield stress, Y_{sat} and C are material parameters of the Voce law. Since the uniaxial tensile tests are monotonic, the kinematic hardening is not considered in the model. The parameters of the Voce law were obtained from the stress–strain curves (experimental uniaxial tensile tests at 0.1 mm/s of crosshead velocity), which are presented in Fig. 4. The optimization procedure minimizes the difference between predicted and experimental stress–strain curves (Chaparro et al., 2008), leading to the material parameters listed in Table 4, considering the two different values of natural aging time. Fig. 9 presents the stress–strain curve obtained for both values of natural aging time (1 month and 18 months). The comparison between experimental and numerical curves highlights the good agreement between them, with a maximum difference lower than 4%.

The anisotropic behaviour of this aluminium alloy is modelled by the classical Hill'48 yield criterion, with anisotropy parameters *F, G, H,*

Table 4
Parameters of the Voce law used to describe the isotropic hardening of the AA6016-T4 aluminium alloy, considering two different values of natural aging time.

Natural aging time	Y_0 [MPa]	Y_{sat} [MPa]	C
1 month	103.2	289.8	10.30
18 months	129.3	319.3	9.83

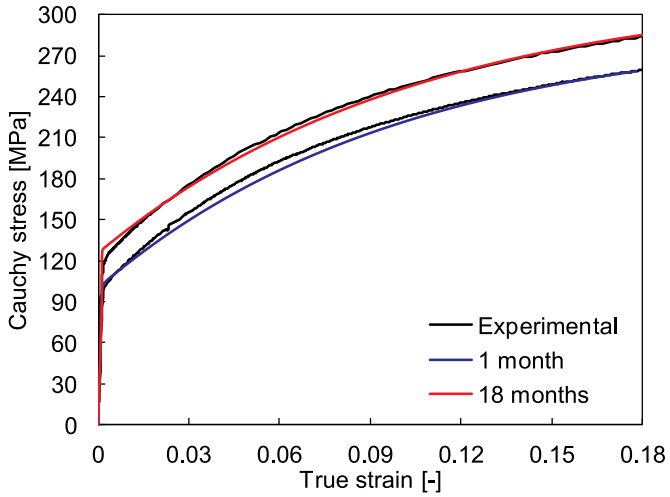

Fig. 9. Comparison between numerical and experimental true stress–true strain curves obtained from uniaxial tensile tests, for 1 month and 18 months of natural aging.

N, L and M (Hill, 1948). The yield surface is considered temperature independent, such as the hardening law. Since the in-plane variation of the flow stress is minor (see Fig. 7) and the planar anisotropy coefficient is negligible (about 0.030) (Simões et al., 2019), planar isotropy is assumed in the yield criterion. Based on the anisotropy coefficients determined by Simões et al. (2019), the normal anisotropy coefficient r, is assumed constant with a value of 0.615. Since the parameters for the Voce law (Table 4) were evaluated from the stress–strain curves obtained in the rolling direction, the conditions $G + H = 1$ is prescribed. Therefore, the anisotropy parameters are calculated using the relations: $F = G = H/r$ and $N = (2r+1)/(r + 1)$. Moreover, the sheet is generally assumed isotropic in the thickness direction due to the difficulties in evaluating the out-of-plane parameters, leading to $L = M = 1.5$, $F = G = 0.625$, $H = 0.375$ and $N = 1.375$. The experimental study of Simões et al. (2019) shows that the impact of the aging time on the anisotropy coefficients is negligible. Thus, the set of parameters defining the planar isotropy is identical for both aging times.

Although the hardening law is strain rate independent, different values of strain rate can be attained in the uniform region of the tensile specimen, depending on the crosshead velocity. The evolution of the predicted strain rate in the midpoint of the tensile specimen is presented in Fig. 10 for the three values of crosshead velocity. The strain rate is approximately constant during the test, i.e. the strain rate is approximately 2×10^{-4} s^{-1}, 2×10^{-3} s^{-1} and 2×10^{-2} s^{-1} assuming 0.01 mm/s, 0.1 mm/s and 1 mm/s for the crosshead velocity, respectively. However, since the onset of necking occurs slightly before the 10 mm of grip displacement, there is a slight increase of the strain rate at the end of the tests, particularly for the 18 months of storage time.

4.2. Transient thermal modelling

The numerical modelling of thermal effects within a solid body requires the solution of a transient heat transfer problem. The variation of the temperature field is defined by the first and second laws of thermodynamics. The differential equation governing the heat transfer within an isotropic and homogeneous body with volume V bounded by a closed surface S assumes the following form:

$$\rho c_p \frac{\partial T}{\partial t} = k\frac{\partial^2 T}{\partial x^2} + k\frac{\partial^2 T}{\partial y^2} + k\frac{\partial^2 T}{\partial z^2} + \dot{w}^p, \tag{2}$$

where ρ is the mass density, c_p represent the specific heat capacity and k denotes the thermal conductivity, which is assumed isotropic. The thermal properties of the aluminium alloy are listed in Table 3. The plastic heat generation rate is denoted by $\dot{w}^p$, which is commonly expressed as a fraction of the plastic work rate, given by:

$$\dot{w}^p = \beta(\boldsymbol{\sigma}: \dot{\boldsymbol{\varepsilon}}^p) \tag{3}$$

where $\boldsymbol{\sigma}$ is the Cauchy stress tensor, $\dot{\boldsymbol{\varepsilon}}^p$ is the plastic strain rate tensor and β is called the Taylor–Quinney coefficient (Taylor and Quinney, 1934), defined in the differential form according to Rittel (1999). This factor is usually assumed constant, ranging between 0.85 and 0.95 for metals (Pereira and Rolfe, 2014). However, some models have been developed in order to define the Taylor–Quinney coefficient as a function of the plastic strain (cf. Section 4.3).

Adiabatic conditions can be assumed in mechanical tests performed under high strain rates conditions (very low loading time), which simplifies the thermo-mechanical analysis of the specimen deformation. Accordingly, the heat conduction term disappears in Eq. (2), leading to:

$$\rho c_p \frac{\partial T}{\partial t} = \beta(\boldsymbol{\sigma}: \dot{\boldsymbol{\varepsilon}}^p), \tag{4}$$

from which β can be experimentally evaluated based on the evolution of the temperature, stress and plastic strain as a function of the time. However, since the strain rate is relatively low in the quasi-static uniaxial tensile tests, it is necessary to model the heat losses and the transient heat conduction. Therefore, the process cannot be modelled as adiabatic and the convection heat loss must be taken into account, in addition to the general heat conduction equation. The convection term, specified on the boundary surface, is defined by:

$$\dot{q} = h(T - T_\infty), \tag{5}$$

where h denotes the convective heat transfer coefficient while T_∞ is the environment temperature. The effect of radiation can be neglected at near room temperature. On the other hand, the heat flow across the contact surface between solids is important in the temperature distribution. The thermal contact between two solids is always imperfect due to the existence of impurities, roughness, etc. Thus, in order to avoid the simulation of an assembly, this heat loss is usually modelled as convection on the contact interface:

$$\dot{q}_c = h_c(T - T_{grip}), \tag{6}$$

where h_c is the interfacial heat transfer coefficient (also called thermal contact conductance), while T_{grip} is the temperatures of the grip surface.

During the uniaxial tensile test, the outer surface of the specimen located in the gauge section is exposed to the surrounding air, while the specimen shoulders (enlarged ends) are compressed by the copper grips (see Fig. 2). Therefore, in the proposed model, the in-plane specimen surface is divided into two regions, as illustrated in Fig. 11, allowing the application of distinct thermal boundary conditions. Since the tests are carried at room temperature ($T_\infty = 22$ °C) in a closed chamber, the specimen surface exposed to air is subjected to natural convection. The convective heat transfer coefficient involved in Eq. (5) is assumed constant and identical for the top and bottom surfaces of the specimen since any difference in the buoyancy force, moving the air around each surface, can be neglected. Regarding the heat loss to the grips, experimental studies show that the interfacial heat transfer coefficient, involved in Eq. (6), depends on several factors, such as surface roughness, material properties, contact pressure, amongst others (Abdollahi et al., 2017; Tariq and Asif, 2016). However, in the present study, the

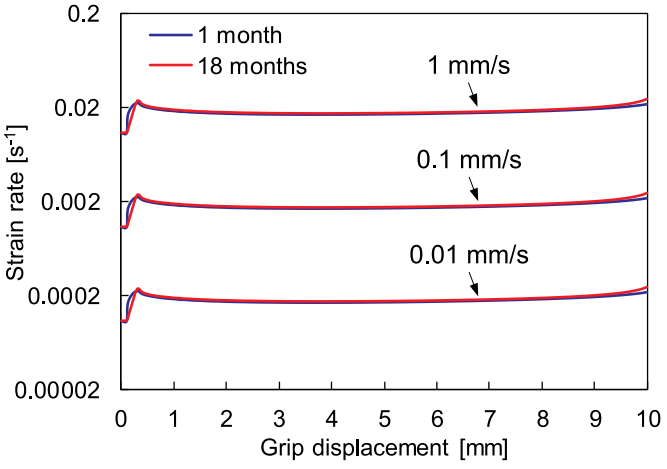

Fig. 10. Predicted strain rate in the midpoint of the tensile specimen, assuming three different values of crosshead velocity, for 1 month and 18 months of natural aging.

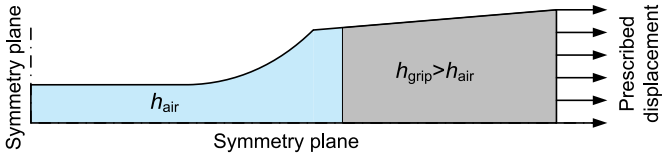

Fig. 11. Definition of the thermal/mechanical boundary conditions on the specimen (one eighth). Identification of the surface area exposed to natural convection and the area in contact with the grip.

interfacial heat transfer coefficient is assumed constant on the specimen surface covered by the grips (see Fig. 11), as suggested by Kardoulaki et al. (2014). The grips temperature is assumed constant and equal to the environment temperature (T_{grip} = 22 °C).

4.3. Taylor–Quinney coefficient

Although the Taylor–Quinney coefficient (β) is generally assumed constant and close to 0.9, the review performed by Macdougall (2000) shows that it can range between 0.12 and 1.0, for different materials. The influence of the plastic strain on the Taylor–Quinney coefficient has been modelled mainly by two theories, describing distinct mechanisms to store the energy in the material. The model developed by Zehnder (1991) takes into account the dislocation density, which increases with the strain evolution (rise rate proportional to the work hardening exponent). Then, the fraction of energy dissipated as heat increases with the strain rise, i.e. the β coefficient increases with the plastic strain. The second model, proposed by Aravas et al. (1990), assumes that the energy stored in the material is associated with residual stresses generated in the metal after plastic deformation. Therefore, the fraction of energy dissipated as heat, given by the β coefficient decreases with the strain rise.

Considering the commercially pure titanium, the comparison between numerical and experimental temperature evolutions carried out by Pottier et al. (2013) shows that the best fit is obtained when the β coefficient increases with the plastic strain, which is in accordance with the Zehnder model. An identical solution was obtained by Fekete and Szekeres (2015) for two different steels. On the other hand, using the uniaxial tension test of a slender rod, (Knysh and Korkolis, 2015) reported that the β coefficient decreases as the plastic deformation accumulates (for two stainless steels and two different titanium alloys), which is consistent with the Aravas model. In order to compare different evolutions for the Taylor–Quinney coefficient used in the present numerical model, both the Zehnder model and the Aravas model are considered, in addition to constant values of β.

The variation of β with the plastic strain, proposed by Zehnder (1991), is expressed as:

$$\beta = 1 - n(\bar{\varepsilon}^{p}/\varepsilon_0)^{n-1}, \tag{7}$$

where n is the strain hardening exponent according to the isotropic hardening law $\sigma = \sigma_0(\bar{\varepsilon}^{p}/\varepsilon_0)^n$ for the plastic regime, where σ_0 and ε_0 denote the yield stress and the yield strain, respectively. Therefore, materials with low strain hardening (lower n) exhibit globally high values of β. Regarding the Aravas model (Aravas et al., 1990), the evolution of the β coefficient with the plastic strain is given by:

$$\beta = 1 - \frac{An - 1 - n}{A - 1 - n}, \tag{8}$$

where

$$A = 2\frac{(\varepsilon/\varepsilon_0)^{1+n} - 1}{(\varepsilon/\varepsilon_0)^{2n} - 1}, \tag{9}$$

where ε is the true strain and the other parameters involved are identical to the ones used in the Zehnder model. Adopting this model, materials with low strain hardening (lower n) exhibit globally high values of β, behaviour also provided by the Zehnder model.

Since the hardening law adopted in this study to describe the mechanical behaviour of the AA6016-T4 aluminium alloy differs from the one considered in the development of the Zehnder and the Aravas models, the parameters involved in (7)–(9) are evaluated by curve fitting. The experimental data from the aluminium alloy with 18 months of natural ageing is used in the fitting procedure, resulting in the parameters n = 0.260 and ε_0 = 0.0066. Considering the aluminium alloy under analysis, Fig. 12 presents the evolution of the β coefficient defined by the Zehnder model (increasing) and by the Aravas model (decreasing). Note that the maximum value of true strain attained in the uniaxial tensile test is approximately 18%, as shown in Fig. 4.

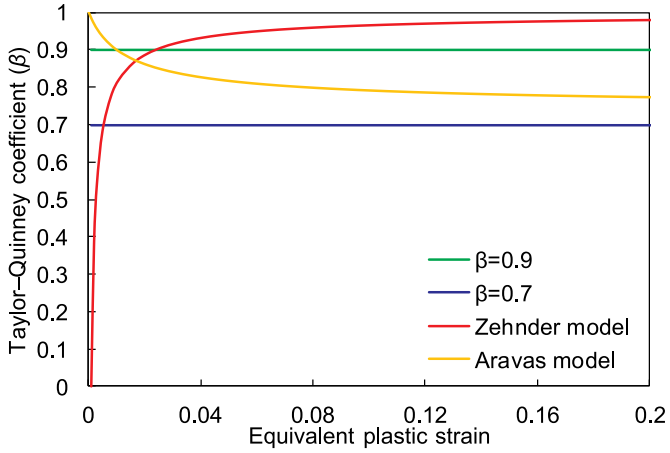

Fig. 12. Fraction of plastic work converted into heat as a function of plastic strain. Comparison of constant values of β with the Zehnder and the Aravas models, calibrated for the aluminium alloy under analysis (18 months of natural aging).

5. Modelling results and analysis

5.1. Uniaxial tensile tests

The temperature in the specimen volume is defined by the balance between the amount of heat generated, the heat conduction and the heat losses. The heat losses are first analysed in this section, namely the ones due to natural convection and due to contact conductance with the grips, which are defined by the natural convective heat transfer coefficient (h_{air}) and the interfacial heat transfer coefficient (h_{grip}), respectively. Regarding the natural convective heat transfer coefficient, the review carried out by Khalifa (2001) highlights that large discrepancies can occur in the experimental values determined by different authors. The study performed by Awbi (1998) uses a chamber to experimentally evaluate the natural convection heat transfer coefficients of a heated wall, a heated floor and a heated ceiling. Since the uniaxial tensile tests are carried in a closed chamber (see Section 2), the values reported in that study will be adopted in the present model, ranging between 1 W/(m^{2}K) and 5 W/(m^{2}K).

It is difficult to evaluate experimentally the interfacial heat transfer coefficient, which dictates the heat exchange between the tensile specimen and the grips (Rosochowska et al., 2004). On the other hand, the range of values reported in the literature is very wide and typically defined as a function of temperature and contact pressure (Caron et al., 2013). The interfacial heat transfer coefficient was recently characterized by Omer et al. (2019) for the 6xxx series aluminium alloys. The values exhibited significant variation with the contact pressure, ranging from 800 W/(m^{2}K) at 2 MPa to 2700 W/(m^{2}K) at 80 MPa. Therefore, such as for the natural convective heat transfer coefficient (h_{air}), different values of interfacial heat transfer coefficient (h_{grip}) are adopted in the numerical simulation, ranging between 800 W/(m^{2}K) and 2700 W/(m^{2}K).

Fig. 13 shows the predicted temperature rise at the midpoint of the specimen during the uniaxial tensile test, performed at three different values of crosshead velocity, comparing 1 month and 18 months of natural aging. The Taylor–Quinney coefficient is assumed constant in this analysis, β=0.9, which is the value used by default in several commercial finite element code packages (Abaqus 2016). On the other hand, different values of convective heat transfer and interfacial heat transfer coefficients are adopted in the numerical model. Whatever the values considered for the heat transfer coefficients (h_{air} and h_{grip}), the same global trend for the temperature rise is predicted by the numerical

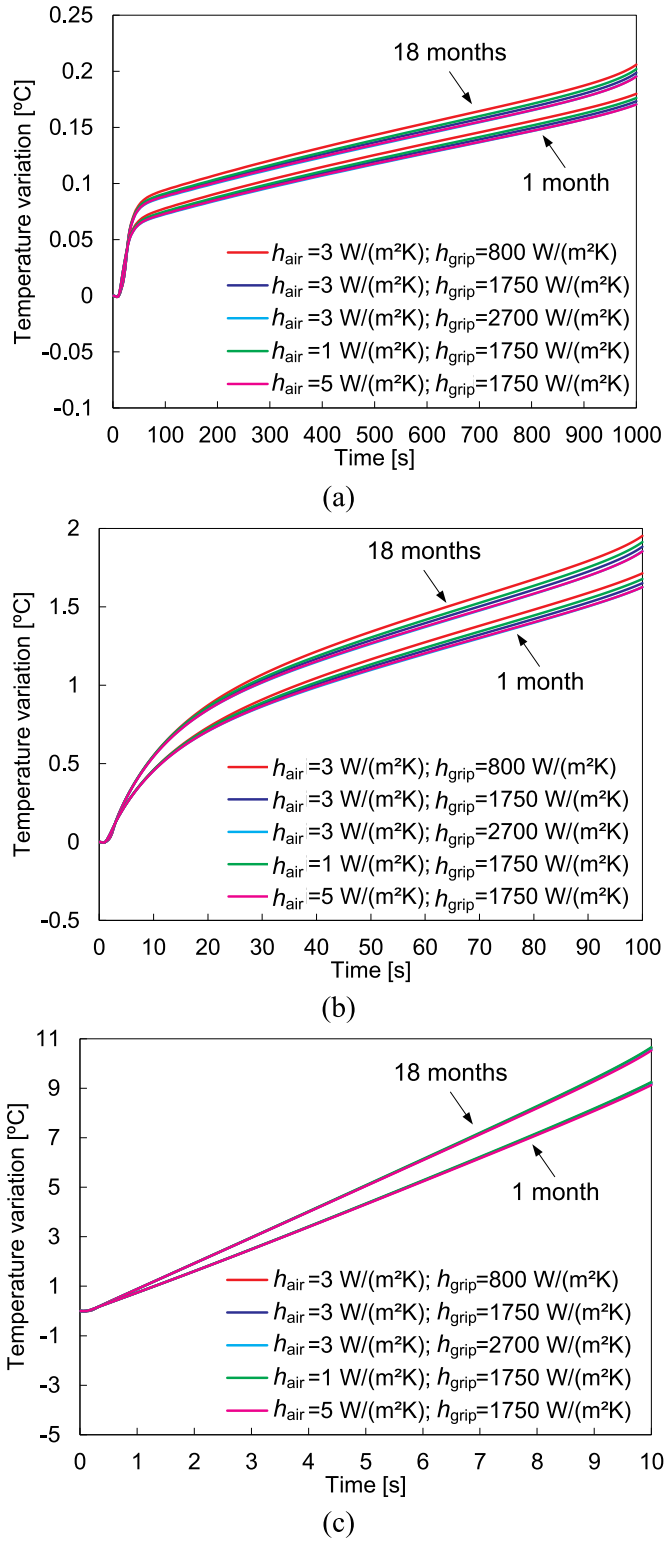

Fig. 13. Evolution of the temperature variation at the midpoint of the specimen for different values of h_{air} and h_{grip}, assuming $\beta = 0.9$: (a) 0.01 mm/s of crosshead velocity; (b) 0.1 mm/s of crosshead velocity; (c) 1 mm/s of crosshead velocity.

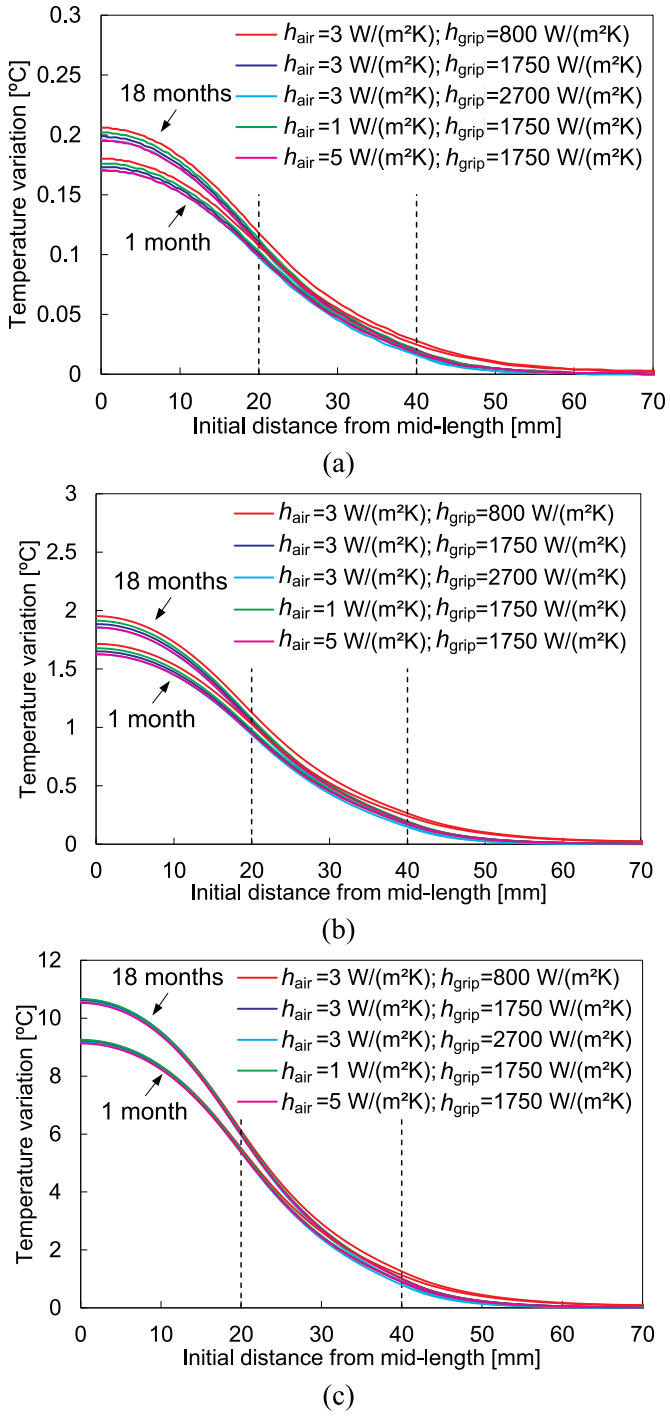

Fig. 14. Distribution of the temperature variation along the specimen length, predicted for a grip displacement of 10 mm using different values of h_{air} and h_{grip}, assuming $\beta = 0.9$: (a) 0.01 mm/s of crosshead velocity; (b) 0.1 mm/s of crosshead velocity; (c) 1 mm/s of crosshead velocity.

model, which is dictated mainly by the crosshead velocity. Adopting different values for the heat transfer coefficients (h_{air} and h_{grip}), the difference in the predicted temperature at the midpoint of the specimen increases during the stretching, but it is always lower than 0.1 ˚C (see Fig. 13). On the other hand, since the natural aging leads to an increase of the material strength (see Fig. 9), the predicted temperature variation is higher for the 18 months of storage time, as shown in Fig. 13. Moreover, the predicted temperature variation increases slightly at the end of the tensile test, when considering 18 months of storage time, since the strain rate also increases at the same instant (Fig. 10). The impact of the natural aging time on the predicted temperature variation after 10 mm of grip displacement, at the midpoint of the specimen, is 0.026 ˚C, 0.23 ˚C and 1.4 ˚C, for 0.01 mm/s, 0.1 mm/s and 1 mm/s of crosshead velocity, respectively. This represents an increase of 15% in the temperature variation (the difference between actual and initial

temperature), comparing 1 month and 18 months of natural aging. Note that, for the numerical results, the increase of the storage time from 1 month to 18 months leads to an increase of the flow stress curve (Fig. 9) between 10% and 25%, depending on the plastic strain value.

The numerical distribution of the temperature variation along the length of the specimen for a grip displacement of 10 mm is presented in Fig. 14, for three values of crosshead velocity and comparing 1 month and 18 months of natural aging. Since the plastic strain occurs predominantly in the uniform section of the specimen, the heat is generated mainly in this zone. However, the heat losses occur predominantly in the contact interface with the grips, leading to a temperature distribution that follows a Gaussian profile (see Fig. 14). The temperature gradient along the specimen gauge section is mainly dictated by the crosshead velocity because the heat losses are directly proportional to the stretching time. Indeed, considering the lowest crosshead velocity, the temperature gradient along the specimen is lower than 0.2 °C (see Fig. 14(a)) due to the long stretching time (1000 s). Considering a specific value for the crosshead velocity, the influence of the heat transfer coefficients (h_{air} and h_{grip}) on the predicted temperature distribution is lower than 0.1 °C in the gauge section, as shown in Fig. 14. In fact, for all crosshead velocities considered, the impact of the heat transfer coefficients on the predicted temperature is within the noise range observed in the experimental data (see Section 3.1). Therefore, considering realistic values for the heat transfer coefficients (h_{air} and h_{grip}), the predicted temperature is roughly independent of the selected values, as highlighted in Fig. 13 and Fig. 14. Therefore, both the natural convective heat transfer coefficient ($h_{air}=3$ W/(m^{2}K)) and the interfacial heat transfer coefficient ($h_{grip}=1750$ W/(m^{2}K)) are assumed constant henceforward.

Fig. 15 presents the comparison between the experimental and predicted temperature rise measured in three locations (TC1, TC3 and TC4) during the uniaxial tensile test with 0.1 mm/s of crosshead velocity, considering four different conditions for the β coefficient (see Fig. 12). Besides, the presented experimental temperature variation is the smoothed average curve of the raw data shown in Fig. 6(b), which is a procedure commonly adopted (Rittel et al., 2017). Since the Joule–Thomson effect (temperature variations due to elastic deformation) is neglected in the present model, the numerical simulation is unable to predict the temperature decrease observed experimentally in the elastic state (0.25 °C). On the other hand, the predicted temperature growth is significantly influenced by the evolution of β coefficient with the plastic strain, as highlighted in Fig. 15.

In order to quantify the discrepancy between numerical and experimental temperature variation, the absolute error of the numerical solution in each time instant can be defined by:

$$\delta T(t) = \Delta T_{num}(t) - \Delta T_{exp}(t) - \Delta T_{elastic}, \quad (10)$$

where $\Delta T_{num}(t)$ and $\Delta T_{exp}(t)$ denote the numerical and experimental temperature variation at instant t, respectively. Since the focus of this study is the analysis of the heat generated by plastic deformation, the error defined by Eq. (10) includes a term related with the thermo-elastic cooling, i.e. the temperature deviation (decrease) from room temperature denoted by $\Delta T_{elastic}$.

The error between experimental and predicted temperature variation is presented in Fig. 16, comparing different values of β coefficient, for 0.1 mm/s of crosshead velocity. The error is evaluated in two locations (TC1 and TC4), corresponding to the thermocouples with maximum and minimum values of temperature variation (see Fig. 6(b)). Globally, the error in the temperature variation is lower when considering the Zehnder model, which is always inferior to 0.2 °C for both locations (see Fig. 16). Besides, since the error value is roughly constant during the stretching, then the trend (slope) of the experimental temperature variation is accurately predicted by the numerical simulation performed with the Zehnder model. On the other hand, $\beta=0.7$ yields the maximum temperature variation error, which is around 0.7 °C in TC1 (see Fig. 16(a)), as well as the largest range during the test (from

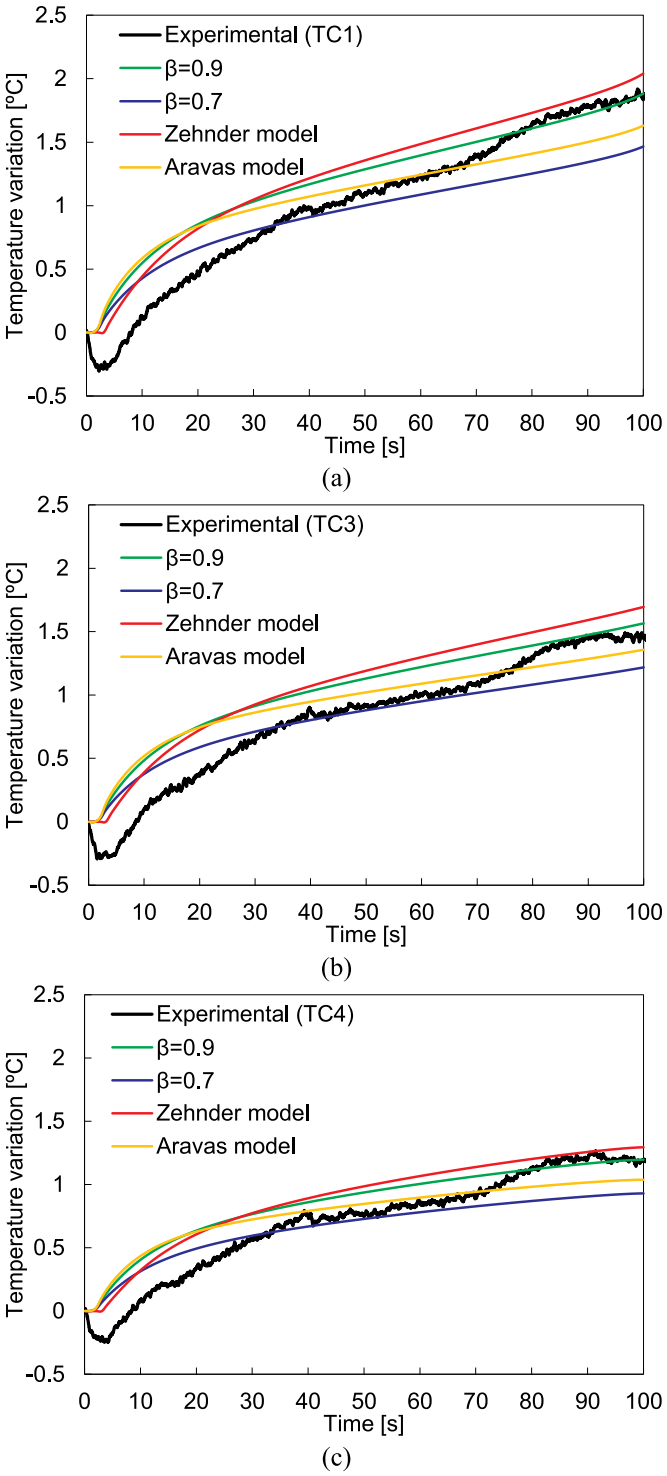

Fig. 15. Experimental and predicted temperature variation for 0.1 mm/s of crosshead velocity, using different values of Taylor−Quinney coefficient and assuming $h_{air}=3$ W/(m^{2}K) and $h_{grip}=1750$ W/(m^{2}K), evaluated in three locations: (a) TC1; (b) TC3; (c) TC4.

−0.7 °C up to 0.2 °C). Therefore, the accurate prediction of the heat generated by plastic deformation requires an increasing evolution of the β coefficient with the plastic strain. Although the temperature variation error is slightly lower for $\beta=0.9$, the results show that considering a constant value for the β coefficient it is impossible to obtain numerically the experimental trend of the temperature rise, even taking into account the Joule–Thomson effect. Comparing the Zehnder and the

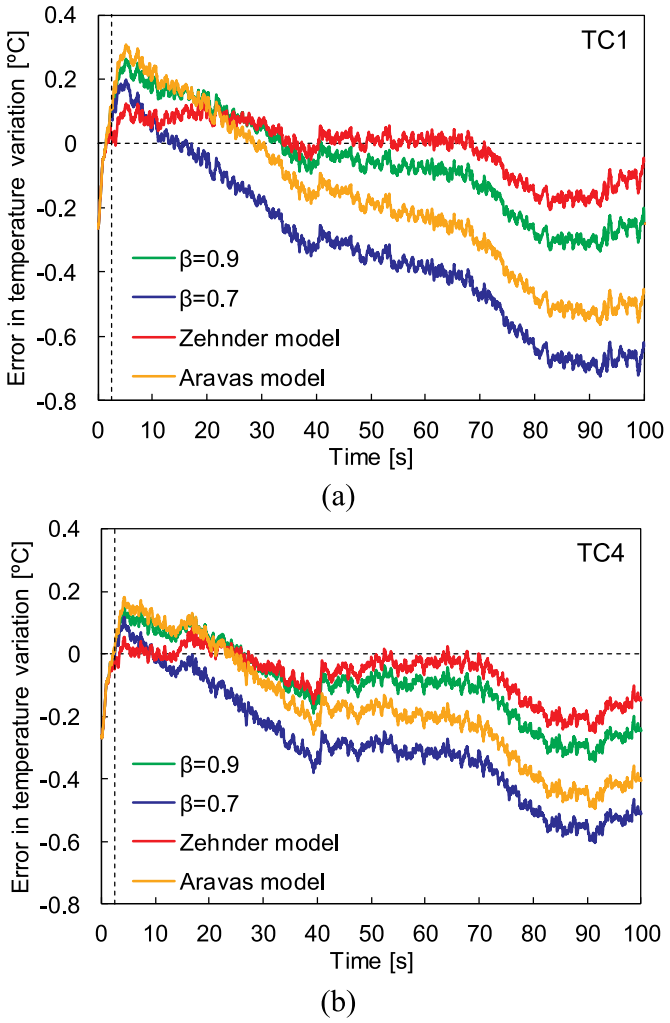

Fig. 16. Error between experimental and predicted temperature variation for 0.1 mm/s of crosshead velocity, using different values of Taylor – Quinney coefficient and assuming $h_{air} = 3$ W/(m^{2}K) and $h_{grip} = 1750$ W/(m^{2}K), evaluated in two locations: (a) TC1; (b) TC4. The vertical dashed line marks the transition between the elastic and the elastoplastic regimes.

Aravas model, the difference between numerical and experimental temperature is lower using the Zehnder model, if the temperature is adjusted to take into account the Joule–Thomson effect. This conclusion is valid for the three locations where the temperature is compared (TC1, TC3 and TC4, as shown in Fig. 15).

The comparison between experimental and predicted temperature variation, measured in three different locations (TC1, TC3 and TC4) during the uniaxial tensile test is presented in Fig. 17, for 1 mm/s of crosshead velocity and considering four different conditions for the β coefficient (see Fig. 12). The experimental temperature variation is the smoothed average curve of the raw data shown in Fig. 6(c). The temperature is globally overestimated for the three locations, except when the β coefficient is 0.7, which provides a solution that overestimates the temperature at the beginning and underestimates it at the end of the tensile test (see Fig. 17).

The error between experimental and predicted temperature variations, defined by Eq. (10), is presented in Fig. 18 for 1 mm/s of crosshead velocity, comparing different values of β coefficient. The error evaluated in the two locations (TC1 and TC4) presents a similar behaviour, i.e. regardless of the model adopted to define the β coefficient, the evolution of the temperature variation error is similar in TC1 (Fig. 18(a)) and TC4 (Fig. 18(b)). However, since the temperature rise is lower in TC4 in comparison with TC1 (see Fig. 17), the error is slightly

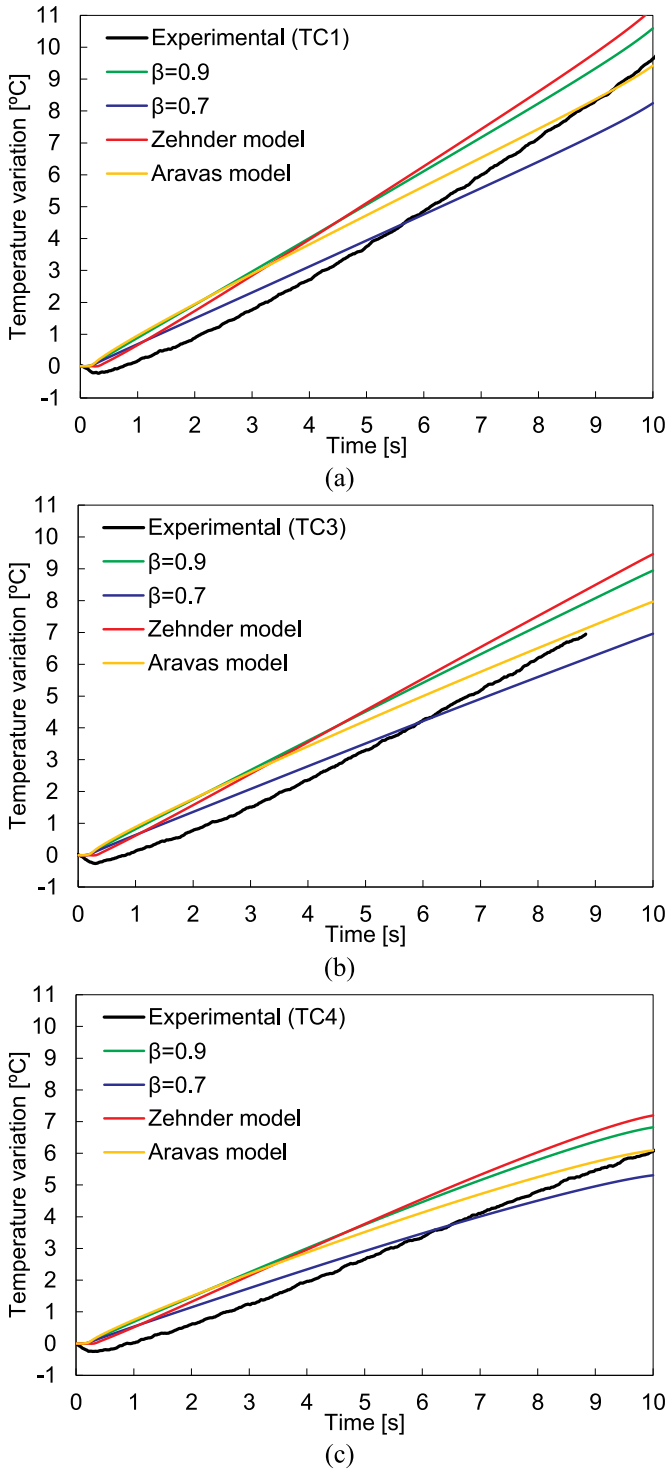

Fig. 17. Experimental and predicted temperature variation for 1 mm/s of crosshead velocity, using different values of Taylor – Quinney coefficient and assuming $h_{air} = 3$ W/(m^{2}K) and $h_{grip} = 1750$ W/(m^{2}K), evaluated in three locations: (a) TC1; (b) TC3; (c) TC4.

lower in TC4 in comparison with TC1, as shown in Fig. 18. Globally, the Zehnder model leads to the highest overestimation of the temperature variation, with an error lower than 1.3 °C in TC1 and lower than 1.0 °C in TC4. Moreover, the absolute error of the numerical solution increased up to 5 times when the crosshead velocity increased from 0.1 mm/s to 1 mm/s (compare Figs. 16 and 18). This increase of the absolute error is the consequence of the predicted temperature variation, which increases approximately 5 times when the crosshead

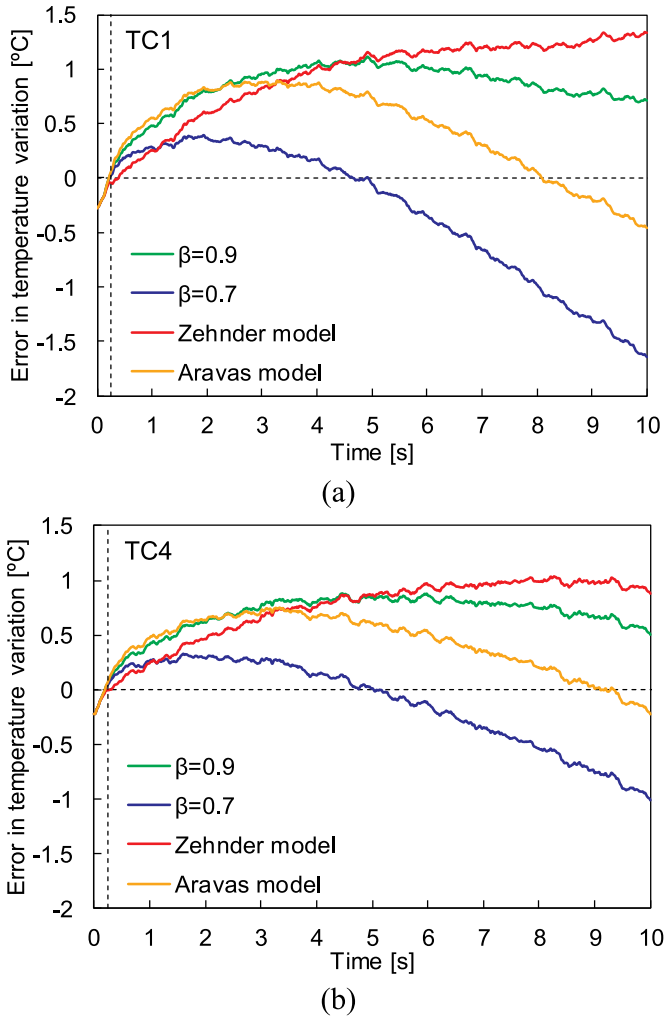

Fig. 18. Error between experimental and predicted temperature variation for 1 mm/s of crosshead velocity, using different values of Taylor – Quinney coefficient and assuming $h_{air} = 3$ W/(m^{2}K) and $h_{grip} = 1750$ W/(m^{2}K), evaluated in two locations: (a) TC1; (b) TC4. The vertical dashed line marks the transition between the elastic and the elastoplastic regimes.

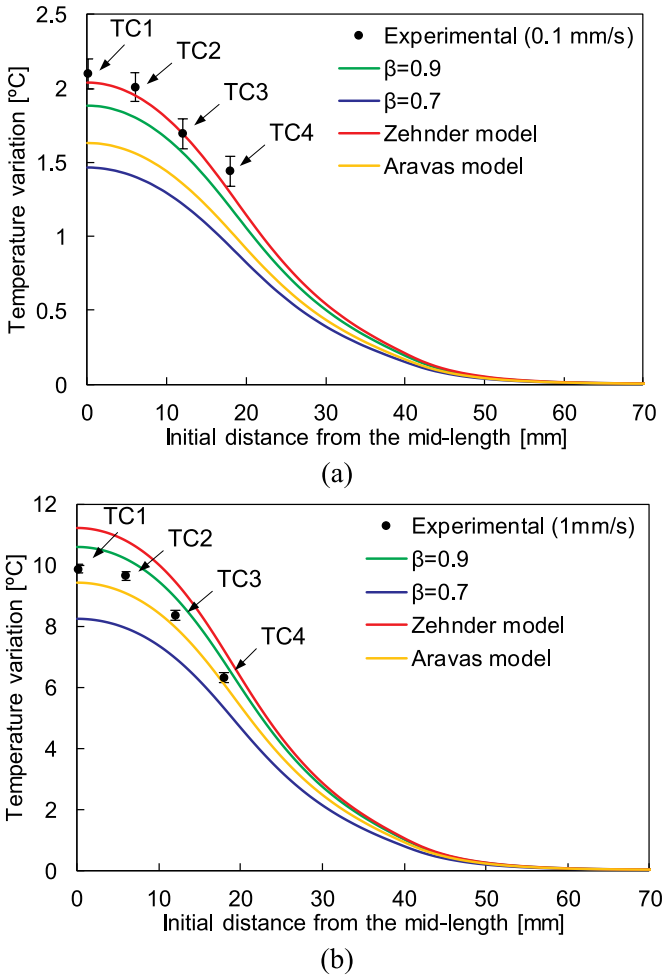

Fig. 19. Distribution of the temperature variation along the specimen length (10 mm of grip displacement) using different values of Taylor – Quinney coefficient and assuming $h_{air} = 3$ W/(m^{2}K) and $h_{grip} = 1750$ W/(m^{2}K): (a) 0.1 mm/s of crosshead velocity; (b) 1 mm/s of crosshead velocity. The experimental values were corrected considering the thermo-elastic cooling, i.e. a $\Delta T_{elastic} = 0.25°C$ was added.

velocity changes from 0.1 mm/s to 1 mm/s. Thus, for the higher crosshead velocity, the influence of the Taylor–Quinney coefficient on the predicted temperature variation is significant, reaching 3 °C. Despite the temperature is globally overestimated in the elastoplastic regime, when assuming $\beta = 0.9$ and by the Zehnder model, the experimental trend for the temperature variation is accurately predicted (almost constant error in the temperature variation), particularly for the last half period of the test.

Based on the preceding comparative analysis, the accurate prediction of the temperature rise requires an increasing evolution of the β coefficient with the plastic strain, which is the basis of the Zehnder model. Taking into account the evolution of the error in the temperature variation presented in Fig. 18, the fraction of plastic work converted into heat should be small for small values of plastic strain and large for large values of plastic strain. However, the evolution of the β coefficient defined by the Zehnder model, using the parameters calibrated from the material hardening law, leads to an overestimation of the β coefficient for small values of plastic strain. Thus, the accuracy of the numerical solution can be improved by reducing the strain hardening exponent involved in Eq. (7), which would generate a slower increase of the β coefficient with the plastic strain compared with the one presented in Fig. 12. Indeed, the experimental strain hardening exponent ($n_{4\text{-}6} = 0.29$) of this aluminium alloy is larger for reduced values of plastic strain (4 – 6%) than for higher values (10–15%; $n_{4\text{-}6} = 0.25$), as shown in Table 2. However, this behaviour is not accurately described by the hardening law that is behind the Zehnder model, which uses a constant value of strain hardening exponent (n). Therefore, the definition of the β coefficient evolution should take into account a more accurate description of the work hardening.

The distribution of the temperature variation along the specimen length is presented in Fig. 19 for the instant corresponding to 10 mm of grip displacement, using different values of the Taylor – Quinney coefficient. The numerical solutions are compared with the experimental one for the tests performed at 0.1 and 1 mm/s of crosshead velocity, which was evaluated only in the four locations (TC1, TC2, TC3 and TC4). The temperature variation profile obtained numerically presents the maximum at the midpoint of the specimen and the minimum in the region in contact with the grips. Although the minimum is identical for all models (dictated by the grips temperature), the maximum value of the temperature variation is influenced by the model adopted to define the β coefficient, because the heat is generated mainly in the uniform section of the specimen. It should be mentioned that the temperature profile evaluated at the end of the tensile test is the result of the entire evolution of the temperature variation, previously shown in Figs. 15 and 17. Thus, using only these results to assess the accuracy of the model can lead to improper conclusions.

Nevertheless, the predicted profile for the temperature variation is globally in good agreement with the experimental one. The error bars shown in Fig. 19 denote the noise amplitude of the experimental temperature measurements, which were corrected considering the thermo-elastic cooling.

Although the temperature variation during the test is accurately predicted using the Zehnder model for 0.1 mm/s of crosshead velocity (Fig. 16), the temperature is globally overestimated for 1 mm/s of crosshead velocity (Fig. 18). The strain rate in the uniform region of the specimen is approximately $2 \times 10^{-3}\ s^{-1}$ for 0.1 mm/s of crosshead velocity and about $2 \times 10^{-2}\ s^{-1}$ for 1 mm/s of crosshead velocity (see Fig. 10). Therefore, the improvement of the numerical solution seems to require an evolution of the β coefficient with the strain rate, in addition to its evolution with the plastic strain (increasing). Indeed, the analysis of the evolution of the error in the temperature variation (Figs. 16 and 18) suggests a negative strain rate sensitivity of the β coefficient, i.e. the β coefficient decreases with the increase of the strain rate. This behaviour is in agreement with the results reported by Knysh and Korkolis (2015) for the stainless steel 316, for which the β coefficient drops as the strain rate increases over a range from $1 \times 10^{-3}\ s^{-1}$ to $1 \times 10^{-2}\ s^{-1}$. The strain rate sensitivity of the β coefficient is commonly related to the mechanical behaviour of the material. However, as shown in Fig. 4, the aluminium alloy under analysis presents no strain rate sensitivity of the flow stress at room temperature.

Recently, some authors showed that the fraction of plastic work converted to heat depends on the deformation mechanisms: twinning and dislocation slip (Kingstedt and Lloyd, 2019). They show that specimens where twinning is highly active during plastic deformation exhibited a lower β coefficient, in comparison with specimens where dislocation slip is the primary source of plastic deformation. Nevertheless, Face Cubic Centred materials with medium-to-high Stacking Fault Energy, such as Aluminium, usually do not deform by twinning, except when the grain size decreases to nanoscale (Jo et al., 2014). Thus, considering the average grain size diameter of the material under study (around 32 μm in Fig. 1), it can be assumed that the predominant deformation mechanism is dislocation slip, whatever the test conditions. In that context, any sensitivity of the Taylor-Quinney coefficient to the strain rate seems to be related to the evolution of the dislocation density. Thus, although the mechanical behaviour observed during the test presents a negligible influence of the strain rate and of the temperature increase, it seems that the strain rate can somewhat affect the proportionality constant of the Zehnder model (assumed equal to one in Eq. (7)).

5.2. Stress relaxation tests

The tensile stress relaxation test was selected to validate the presented finite element model. The numerical simulations were performed considering the same four different conditions for the β coefficient (see Fig. 12). Regarding the heat losses, both the natural convective heat transfer coefficient ($h_{air} = 3$ W/(m^{2}K)) and the interfacial heat transfer coefficient ($h_{grip} = 1750$ W/(m^{2}K)) are assumed constant. Fig. 20 presents the comparison between the numerical and the experimental values of elongation measured in three different regions of the specimen (gauge section). The imposed crosshead displacement was adjusted to fit the experimental elongation values measured during the whole relaxation test, as shown in Fig. 20. Accordingly, the real crosshead velocity used in the finite element model is 0.097 mm/s, which is assumed constant during each stretching period. During the stretching, the experimental elongation presents a slight deviation in relation to the linear increase (particularly in the third loading stage), which is a consequence of the Lüders bands that occur on this material at room temperature (Simões et al., 2019).

The comparison between experimental and numerical temperature variation during the tensile stress relaxation test is presented in Fig. 21, evaluated in four locations (TC1, TC2, TC3 and TC4). The temperature

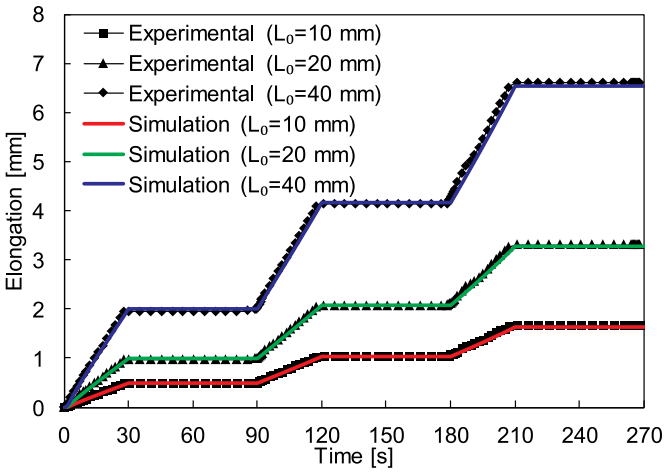

Fig. 20. Experimental and numerical elongation measured in different regions of the specimen during the tensile stress relaxation test.

increases during the stretching since the heat generated by plastic deformation is higher than the heat losses to the environment and grips. On the other hand, temperature decreases during the stress relaxation period due to the heat losses to the environment and to the grips, converging to the room temperature, as shown in Fig. 21. Since the strain hardening leads to an increase of the yield stress with the plastic strain (see Fig. 4), the temperature rise is largest in the last loading cycle. The temperature evolution (rise and decrease) is properly predicted by all numerical models, including the temperature gradient along the specimen length. Globally, the Zehnder model and the constant value of Taylor–Quinney coefficient $\beta = 0.9$ predict the highest temperature variation. The maximum difference in the temperature variation obtained by the different models occurs in the last loading cycle, which is approximately 0.5 °C in TC1 and 0.3 °C in TC4, as shown in Fig. 21. Considering the thermo-elastic cooling (0.25 °C), i.e. imposing a shift down of the numerical curves, the error in the temperature variation is lower for the Zehnder model. However, when comparing the Zehnder model with the constant value of Taylor–Quinney coefficient $\beta = 0.9$, the highest difference in the predicted temperature variation is about 0.1 °C. Thus, it is not possible to state that the Zehnder model leads to better results. The results also highlight that most of the plastic work is converted into heat. Since the heat generation mechanisms are identical in stress relaxation and uniaxial tensile tests, the conclusions about the predicted temperature variation are also similar.

6. Conclusions

This study presents the analysis of the heat generated by plastic deformation in quasi-static uniaxial tensile tests, comparing experimental and numerical results. The age-hardenable aluminium alloy AA6016-T4 is adopted in the present study, comparing two different values of natural aging time, namely 1 month and 18 months. Although the adopted alloy is strain rate insensitive at room temperature, three different values of crosshead velocity (0.01 mm/s, 0.1 mm/s and 1 mm/s) are used. This allows obtaining distinct values of stretching time and, consequently, different amounts of heat lost to the environment and grips.

The experimental temperature is measured by four thermocouples welded on the specimen surface, recording both the evolution and the distribution. The thermo-elastic cooling of the specimen is observed during elastic straining, leading to a temperature decrease of about 0.25 °C (uniform in the gauge section). Considering 10 mm of grip displacement, the temperature rise at the specimen middle is nearly 2 °C and 10 °C for 0.1 mm/s and 1 mm/s of crosshead velocity,

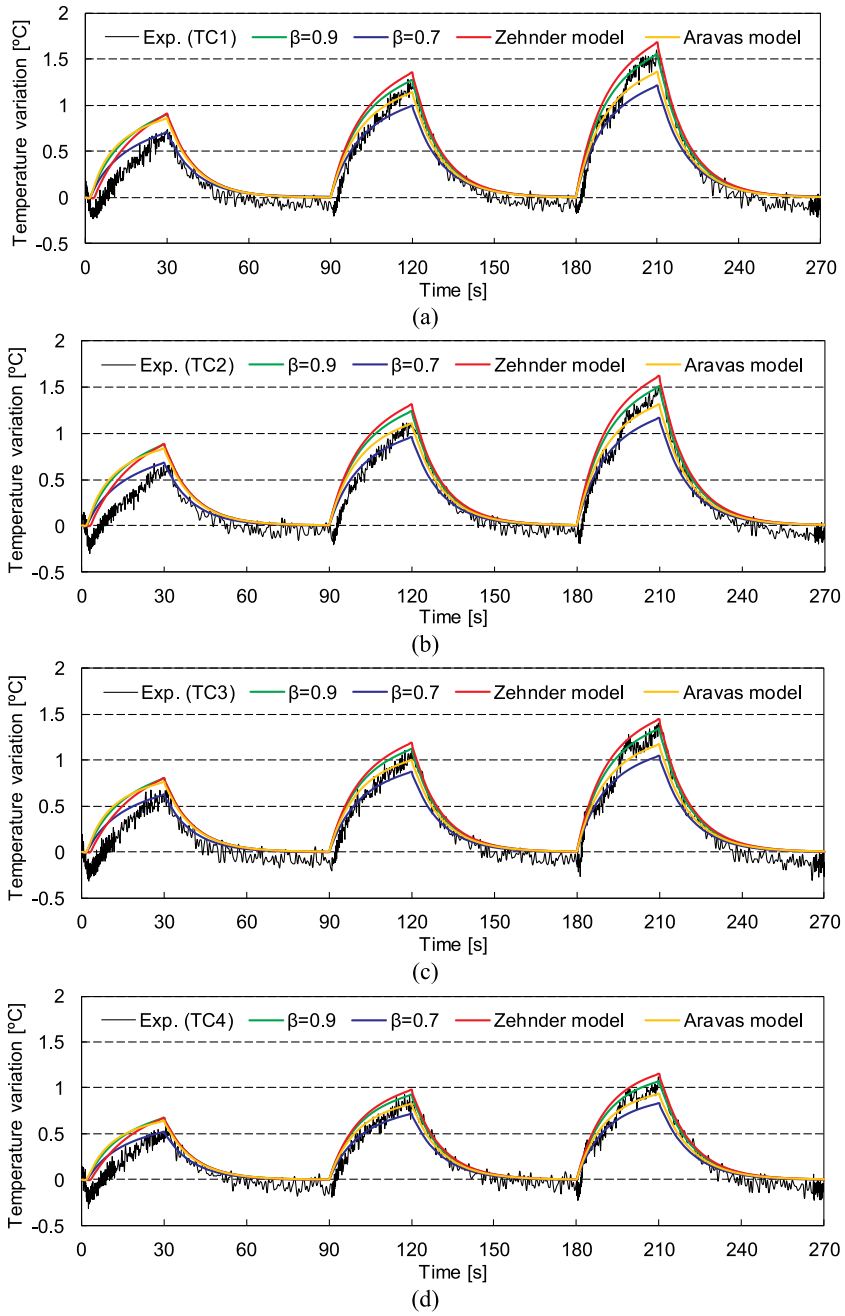

Fig. 21. Experimental and predicted temperature variation during the relaxation test, using different values of Taylor – Quinney coefficient and assuming $h_{air} = 3$ W/(m^{2}K) and $h_{grip} = 1750$ W/(m^{2}K), evaluated in four locations: (a) TC1; (b) TC2; (c) TC3; (d) TC4.

respectively. Besides, the natural aging time leads to an increase of the temperature rise due to the higher flow stress, particularly for 1 mm/s of crosshead velocity.

The presented thermo-mechanical finite element model of the uniaxial tensile test neglects the elastic cooling effect, but takes into account the heat generated by plastic deformation, as well as the heat losses by natural convection and contact conductance. Adopting realistic values for both the natural convective heat transfer coefficient (h_{air}) and the interfacial heat transfer coefficient (h_{grip}), the predicted temperature variation is almost independent of the values selected, i.e. the difference is always lower than 0.1 °C. However, the influence of the Taylor–Quinney coefficient on the predicted temperature is significant, which can reach up to 3 °C for 1 mm/s of crosshead velocity.

Comparing the numerical and experimental evolutions of the temperature variation, the numerical solution is in good agreement with the experimental one, when it is assumed that the fraction of plastic work converted into heat increases as the plastic deformation accumulates. This behaviour is described by the Zehnder model, but the evolution of the Taylor–Quinney coefficient is defined assuming a constant value for the hardening coefficient, which does not fit the hardening behaviour observed for this aluminium alloy. Thus, since the numerical modelling of the stress–strain curves dictate the evolution of the Taylor–Quinney coefficient and, consequently, the obtained temperature prediction, improved relationships should be developed for materials presenting an evolution of the hardening coefficient with the plastic strain. Moreover, the accurate prediction of the temperature rise seems to require a negative strain rate sensitivity of the Taylor–Quinney coefficient, i.e. the Taylor–Quinney coefficient seems to drop when the strain rate increases from 2×10^{-3} s^{-1} up to 2×10^{-2} s^{-1}.

CRediT authorship contribution statement

D.M. Neto: Conceptualization, Methodology, Investigation, Writing - original draft. **V.M. Simões:** Validation, Investigation, Formal analysis, Writing - original draft. **M.C. Oliveira:** Formal analysis, Writing - review & editing, Investigation. **J.L. Alves:** Methodology, Software. **H. Laurent:** Resources, Writing - review & editing, Supervision. **A. Oudriss:** Investigation, Validation. **L.F. Menezes:** Software, Supervision.

Declaration of Competing Interest

Manuscript entitled "Experimental and numerical analysis of the heat generated by plastic deformation in quasi-static uniaxial tensile tests", by D.M. Neto, V.M. Simões, M.C. Oliveira, J.L. Alves, H. Laurent, A. Oudriss and L.F. Menezes. The authors declare no conflicts of interest. The funders had no role in the design of the study; in the collection, analyses, or interpretation of data; in the writing of the manuscript, or in the decision to publish the results.

Acknowledgements

The authors would like to acknowledge the funding from of the Foundation for Science and Technology (FCT) under projects PTDC/EMS-TEC/6400/2014 (POCI-01-0145-FEDER-016876), PTDC/EMS-TEC/0702/2014 (POCI-01-0145-FEDER-016779) and PTDC/EME-APL/29713/2017 (CENTRO-01-0145-FEDER-029713) by UE/FEDER through the program COMPETE 2020. The support under the project MATIS (CENTRO-01-0145-FEDER-000014) and UID/EMS/00285/2020 is also acknowledged.

Supplementary materials

Supplementary material associated with this article can be found, in the online version, at doi:10.1016/j.mechmat.2020.103398.

Appendix A: Temperature measurements

In order to evaluate the uncertainty of the temperature measurements, some of the tensile tests were performed using additional type-K thermocouples with wire diameters of 80 μm. In these tests, four thermocouples of 250 μm and four thermocouples of 80 μm were welded on the specimen surface, side by side in a straight line along the length, according to the procedure shown in Fig. 3. This experimental setup with a total of 8 thermocouples was performed only for the tensile specimens aged for 18 months, at the crosshead velocity of 0.1 mm/s and 1 mm/s. Fig. A.1 compares the evolution of the temperature variation with time, obtained by the thermocouples with different diameters.

Globally, the results show that the temperature variation is only slightly affected by the wire size of the thermocouples. For the same position along the specimen length, the thermocouples with a wire of 80 μm measure a slightly higher temperature variation, for the same time instant. In fact, it is known that the response time of the thermocouples is a function of the wire diameter. The use of the Gleeble machine guarantees the synchronization between the stress-strain results and the temperature evolution. Therefore, it is possible to observe that thermocouples with different wire diameters respond to the beginning of the elastic regime (temperature drop), to the transition to the elastoplastic regime (temperature raise) and to the specimen fracture (temperature drop) at similar instants. This can be observed in Fig. A.1 for both the beginning of the elastic regime and the transition to the elastoplastic one. Since the thermocouples are welded in the specimen surface (exposed), a fast response time was expected (Omega Engineering Inc 2010). The difference in the temperature variation measured by thermocouples with different wire diameters can be a consequence of the response time and precision. Nonetheless, the maximum difference (at the maximal load) in terms of measured temperature variation between thermocouples of wire diameter of 80 μm and 250 μm is inferior to 0.07 °C and 0.4 °C for the crosshead velocity of 0.1 mm/s and 1 mm/s, respectively. It equates to a maximal error of about 4% in the temperature variation. Such difference was considered not relevant to the results discussion, and therefore the authors decide to use thermocouples with a wire diameter of 250 μm since they are easier to apply.

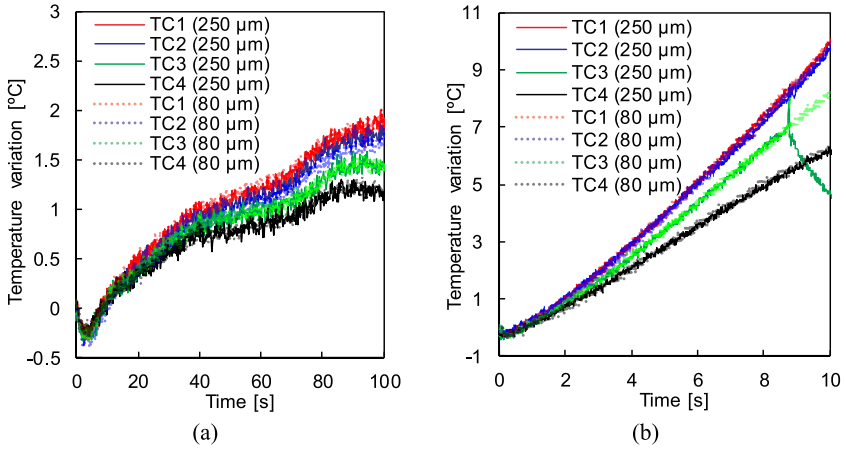

Fig. A.1. Experimental temperature variation, measured by eight thermocouples of type-K, four with a wire diameter of 80 μm and other four with 250 μm in the same specimen:
(a) 0.1 mm/s of crosshead velocity; (b) 1 mm/s of crosshead velocity.

References

Abaqus, 2016. Theory Manual, Version 6.11.

Abdollahi, H., Shahraki, S., Motahari-Nezhad, M, 2017. A review on the effects of different parameters on contact heat transfer. Thermophys. Aeromech. 24, 499–512. https://doi.org/10.1134/S0869864317040011.

Ait-Amokhtar, H., Fressengeas, C., Boudrahem, S, 2008. The dynamics of portevin–le chatelier bands in an Al–Mg alloy from infrared thermography. Mater. Sci. Eng. A 488, 540–546. https://doi.org/10.1016/J.MSEA.2007.11.075.

Aravas, N., Kim, K.-S., Leckie, F.A, 1990. On the calculations of the stored energy of cold work. J. Eng. Mater. Technol. 112, 465. https://doi.org/10.1115/1.2903358.

Awbi, H.B., 1998. Calculation of convective heat transfer coefficients of room surfaces for natural convection. Energy Build. 28, 219–227. https://doi.org/10.1016/S0378-7788(98)00022-X.

Bernard, C., Coër, J., Laurent, H., Chauvelon, P., Manach, P.Y, 2013. Relationship between local strain jumps and temperature bursts due to the portevin-le chatelier effect in an al-mg alloy. Exp. Mech. 53, 1025–1032. https://doi.org/10.1007/s11340-012-9711-4.

Carlomagno, G.M., Cardone, G., 2010. Infrared thermography for convective heat transfer measurements. Exp. Fluids 49, 1187–1218. https://doi.org/10.1007/s00348-010-0912-2.

Caron, E., Daun, K.J., Wells, M.A, 2013. Experimental characterization of heat transfer coefficients during hot forming die quenching of boron steel. Metall. Mater. Trans. B 44, 332–343. https://doi.org/10.1007/s11663-012-9772-x.

Chaparro, B.M., Thuillier, S., Menezes, L.F., Manach, P.Y., Fernandes, J.V, 2008. Material parameters identification: gradient-based, genetic and hybrid optimization algorithms. Comput Mater Sci 44, 339–346. https://doi.org/10.1016/J.COMMATSCI.2008.03.028.

Engler, O., Schäfer, C., Myhr, O.R, 2015. Effect of natural ageing and pre-straining on strength and anisotropy in aluminium alloy aa 6016. Mater. Sci. Eng. A 639, 65–74. https://doi.org/10.1016/J.MSEA.2015.04.097.

Farren, W.S., Taylor, G.I., 1925. The heat developed during plastic extension of metals. Proc. R. Soc. A Math. Phys. Eng. Sci. 107, 422–451. https://doi.org/10.1098/rspa.1925.0034.

Fekete, B., Szekeres, A., 2015. Investigation on partition of plastic work converted to heat during plastic deformation for reactor steels based on inverse experimental-computational method. Eur. J. Mech. A/Solids 53, 175–186. https://doi.org/10.1016/j.euromechsol.2015.05.002.

Gao, Y., Wagoner, R.H., 1987. A simplified model of heat generation during the uniaxial tensile test. Metall. Mater. Trans. A 18, 1001–1009. https://doi.org/10.1007/BF02668548.

GOM mbH. ARAMIS: User Information - Hardware. 2009.

Hazra, S., Williams, D., Roy, R., Aylmore, R., Smith, A, 2011. Effect of material and process variability on the formability of aluminium alloys. J. Mater. Process. Technol. 211, 1516–1526. https://doi.org/10.1016/J.JMATPROTEC.2011.04.001.

Hill, R., 1948. A theory of the yielding and plastic flow of anisotropic metals. Proc. R. Soc. A Math. Phys. Eng. Sci. 193, 281–297. https://doi.org/10.1098/rspa.1948.0045.

Hodowany, J., Ravichandran, G., Rosakis, A.J., Rosakis, P, 2000. Partition of plastic work into heat and stored energy in metals. Exp. Mech. 40, 113–123. https://doi.org/10.1007/BF02325036.

Hughes, T.J.R., 1980. Generalization of selective integration procedures to anisotropic and nonlinear media. Int. J. Numer. Methods Eng. 15, 1413–1418. https://doi.org/10.1002/nme.1620150914.

Jo, M., Koo, Y.M., Lee, B.-J., Johansson, B., Vitos, L., Kwon, S.K, 2014. Theory for plasticity of face-centered cubic metals. Proc. Natl. Acad. Sci. USA 111, 6560–6565. https://doi.org/10.1073/pnas.1400786111.

Kardoulaki, E., Lin, J., Balint, D., Farrugia, D, 2014. Investigation of the effects of thermal gradients present in Gleeble high-temperature tensile tests on the strain state for free cutting steel. J. Strain Anal. Eng. Des. 49, 521–532. https://doi.org/10.1177/0309324714531950.

Khalifa, A.-J.N., 2001. Natural convective heat transfer coefficient – a review: I. Isolated vertical and horizontal surfaces. Energy Convers. Manag. 42, 491–504. https://doi.org/10.1016/S0196-8904(00)00042-X.

Kingstedt, O.T., Lloyd, J.T., 2019. On the conversion of plastic work to heat in mg alloy AZ31B for dislocation slip and twinning deformation. Mech. Mater. 134, 176–184. https://doi.org/10.1016/J.MECHMAT.2019.04.009.

Knysh, P., Korkolis, Y.P., 2015. Determination of the fraction of plastic work converted into heat in metals. Mech. Mater. 86, 71–80. https://doi.org/10.1016/j.mechmat.2015.03.006.

Kuo, T.Y., Lin, H.S., Lee, H.T, 2005. The relationship between of fracture behaviors and thermomechanical effects of alloy AA2024 of T3 and T81 temper designations using the center crack tensile test. Mater. Sci. Eng. A 394, 28–35. https://doi.org/10.1016/j.msea.2004.10.014.

Macdougall, D., 2000. Determination of the plastic work converted to heat using radiometry. Exp. Mech. 40, 298–306. https://doi.org/10.1007/BF02327503.

Manach, P.Y., Coër, J., Jégat, A., Laurent, H., Yoon, J.W, 2016. Benchmark 3 - Springback of an Al-Mg alloy in warm forming conditions. J. Phys. Conf. Ser. 734, 022003. https://doi.org/10.1088/1742-6596/734/2/022003.

Martins, J.M.P., Neto, D.M., Alves, J.L., Oliveira, M.C., Laurent, H., Andrade-Campos, A., et al., 2017. A new staggered algorithm for thermomechanical coupled problems. Int. J. Solids Struct. 122–123. https://doi.org/10.1016/j.ijsolstr.2017.06.002. 42–58.

Mason, J.J., Rosakis, A.J., Ravichandran, G, 1994. On the strain and strain rate dependence of the fraction of plastic work converted to heat: an experimental study using high speed infrared detectors and the Kolsky bar. Mech. Mater. 17, 135–145. https://doi.org/10.1016/0167-6636(94)90054-X.

Menezes, L.F., Teodosiu, C., 2000. Three-dimensional numerical simulation of the deep-drawing process using solid finite elements. J. Mater. Process. Technol. 97, 100–106. https://doi.org/10.1016/S0924-0136(99)00345-3.

Mills, K.C., 2002. Recommended values of thermophysical properties for selected commercial alloys. Woodhead.

Neto, D.M., Martins, J.M.P., Cunha, P.M., Alves, J.L., Oliveira, M.C., Laurent, H., et al., 2018. Thermo-mechanical finite element analysis of the AA5086 alloy under warm forming conditions. Int. J. Solids Struct. 151, 99–117. https://doi.org/10.1016/j.ijsolstr.2017.06.011.

Oliveira, M.C., Alves, J.L., Menezes, L.F, 2008. Algorithms and strategies for treatment of large deformation frictional contact in the numerical simulation of deep drawing process. Arch. Comput. Methods Eng. 15, 113–162.

Omega Engineering Inc, 2010. The Temperature Handbook. Stamford.

Omer, K., Butcher, C., Worswick, M, 2019. Characterization of heat transfer coefficient for non-isothermal elevated temperature forming of metal alloys. Int. J. Mater. Form 1–25. https://doi.org/10.1007/s12289-019-01478-3.

Pandey, K.N., Chand, S, 2003. Deformation based temperature rise: a review. Int. J. Press Vessel Pip 80, 673–687. https://doi.org/10.1016/J.IJPVP.2003.07.001.

Pereira, M.P., Rolfe, B.F., 2014. Temperature conditions during “cold” sheet metal stamping. J. Mater. Process. Technol. 214, 1749–1758. https://doi.org/10.1016/j.jmatprotec.2014.03.020.

Pottier, T., Toussaint, F., Louche, H., Vacher, P, 2013. Inelastic heat fraction estimation from two successive mechanical and thermal analyses and full-field measurements. Eur. J. Mech. A/Solids 38, 1–11. https://doi.org/10.1016/j.euromechsol.2012.09.002.

Revil-Baudard, B., Cazacu, O., Flater, P., Kleiser, G, 2015. Plastic deformation of high-purity ??-titanium: model development and validation using the taylor cylinder impact test. Mech. Mater. 80, 264–275. https://doi.org/10.1016/j.mechmat.2014.03.010.

Rittel, D, 1998. Transient temperature measurement using embedded thermocouples. Exp. Mech. 38, 73–78. https://doi.org/10.1007/BF02321647.

Rittel, D., Zhang, L.H., Osovski, S, 2017. The dependence of the Taylor–Quinney coefficient on the dynamic loading mode. J. Mech. Phys. Solids 107, 96–114. https://doi.org/10.1016/j.jmps.2017.06.016.

Rittel, D., 1999. On the conversion of plastic work to heat during high strain rate deformation of glassy polymers. Mech. Mater. 31, 131–139. https://doi.org/10.1016/S0167-6636(98)00063-5.

Rosochowska, M., Chodnikiewicz, K., Balendra, R, 2004. A new method of measuring thermal contact conductance. J. Mater. Process. Technol. 145, 207–214. https://doi.org/10.1016/S0924-0136(03)00671-X.

Rusinek, A., Klepaczko, J.R., 2009. Experiments on heat generated during plastic deformation and stored energy for trip steels. Mater. Des. 30, 35–48. https://doi.org/10.1016/J.MATDES.2008.04.048.

Simões, V., Laurent, H., Oliveira, M., Menezes, L, 2019. The influence of warm forming in natural aging and springback of Al-Mg-Si alloys. Int. J. Mater. Form 12 (1), 57–68. https://doi.org/10.1007/s12289-018-1406-7.

Simões, V.M., Oliveira, M.C., Laurent, H., Menezes, L.F, 2019. The punch speed influence on warm forming and springback of two Al-Mg-Si alloys. J. Manuf. Process. 38, 266–278. https://doi.org/10.1016/J.JMAPRO.2019.01.020.

Smits, F.M., 1958. Measurement of sheet resistivities with the four-point probe. Bell Syst. Tech. J. 37, 711–718. https://doi.org/10.1002/j.1538-7305.1958.tb03883.x.

Tariq, A., Asif, M., 2016. Experimental investigation of thermal contact conductance for nominally flat metallic contact. Heat Mass Transf. 52, 291–307. https://doi.org/10.1007/s00231-015-1551-1.

Taylor, G.I., Quinney, H., 1934. The latent energy remaining in a metal after cold working. Proc. R. Soc. A Math. Phys. Eng. Sci. 143, 307–326. https://doi.org/10.1098/rspa.1934.0004.

Zehnder, A.T., Babinsky, E., Palmer, T, 1998. Hybrid method for determining the fraction of plastic work converted to heat. Exp. Mech. 38, 295–302. https://doi.org/10.1007/BF02410392.

Zehnder, A.T., 1991. A model for the heating due to plastic work. Mech. Res. Commun. 18, 23–28. https://doi.org/10.1016/0093-6413(91)90023-P.

Zhang, T., Guo, Z.-.R., Yuan, F.-.P., Zhang, H.-.S, 2017. Investigation on the plastic work-heat conversion coefficient of 7075-T651 aluminum alloy during an impact process based on infrared temperature measurement technology. Acta Mech. Sin 1–7. https://doi.org/10.1007/s10409-017-0673-8.